Molecular Profiling of Breast Cancer Cell Lines Containing Amplified Fibroblast Growth Factor Receptors

by

Luke Maggs

MRes Molecular and Cellular Biology

Abstract

Fibroblast Growth Factor Receptor (FGFR) genes 1 and 2 are amplified in a subset of breast cancers. This can lead to overexpression of the receptor at the extracellular membrane resulting in increased ligand independent dimerization and subsequent aberrant signalling involved in the development and progression of the tumour. A SILAC experiment using SU5402 and Dasatinib, FGFR and Src inhibitors respectively was performed on CAL120 breast cancer cells following validation of the function and effectiveness of the inhibitors via western blotting. Increasing our knowledge of the phosphorylation events involved in the signalling pathways affected in breast cancers will produce a molecular map of specific breast cancers allowing more specialised treatment. 340 proteins were found with significantly decreased levels of phosphorylation when cells were treated with SU5402, with MAPK pathway repression. Dasatinib treatment reduced 131 phospho-proteins and suggested components of Src directed cytoskeleton assembly necessary for FGFR transport. Testing of separate FGFR and Src inhibitor effectiveness was also achieved as well as method development of the phosphoenrichment stage of the SILAC experiment. Duplicate SILAC experiments need to be performed to increase the data set and validate findings.

Contents

Introduction

Protein kinases are enzymes which are able to phosphorylate other proteins and can therefore switch a protein from one state to another. Phosphorylation is the addition of a phosphate group to a protein. This modification adds the phosphate group to either a serine, threonine or tyrosine residue on the protein. This is a vital component of the signalling pathway as addition or removal of a phosphate group can change the conformational shape of the protein switching it between either an 'activate' or 'inactive' functional state (Mann et al., 2002). For instance Src contains a SH2 domain which binds specifically to phosphorylated tyrosine residues allowing Src to then become phosphorylated itself and bind substrates it wouldn't have done in its unphosphorylated state. This is an effective way to signal within the cell and pass a communication from protein to protein in order to change activity and function. Tyrosine kinases are a subset of these protein kinases which cause phosphorylation on a tyrosine residue of the protein. Tyrosine kinase receptors are transmembrane receptors at the cell surface which can initiate cell signalling when a ligand binds to their extracellular domain. This triggers activation of the intracellular tyrosine kinase domain which can phosphorylate specific proteins that dock at this site and lead to a cascade of signalling events ultimately affecting cellular processes.

Fibroblast Growth Factors (FGF) are a family of 22 proteins found in mammals, which are involved in both embryonic development and maintaining processes in the adult system. They do this by binding to specific single transmembrane tyrosine kinase receptors known as Fibroblast Growth Factor Receptors (FGFR), at the extracellular membrane. This triggers a number of intricate intracellular signalling pathways resulting in target gene activation or inhibition and production of a cellular response.

FGFR signalling

The 22 distinct FGFs vary in size from 17-34kDa but all share a conserved sequence of 120 amino acids (Eswarakumar et al. 2005). During embryonic development they are involved in cell proliferation, differentiation and migration. Loss of a single FGF has been shown by homologous recombination to usually still produce a viable mouse, but with severe tissue specific defects (Eswarakumar et al. 2005). In the adult they play a role in cellular homeostasis, regulation of angiogenesis and tissue repair. FGFs are secreted and sequestered in the extracellular matrix (ECM) by heparin sulphate proteoglycans (HSPG) (Turner and Grose, 2010). HSPG has a low affinity for FGF compared to FGFR but is important as an accessary protein to regulate FGF binding and receptor activation. In order to signal FGFs act directly on cells from their position in the ECM and are released by proteases which digest the ECM or specific FGF-binding proteins carrying FGF to its target (Powers et al. 2000). This then allows FGF to form a complex with FGFR and HSPG at the cell membrane (Mohammadi et al., 2005).

In humans there are five FGF receptors. FGFRs1-4 are single pass transmembrane tyrosine kinase receptors. FGFR5 lacks the intracellular tyrosine kinase domain and so although it has a high affinity for FGF, its function is not well understood (Brooks et al. 2012). The extracellular portion of each FGFR contains three immunoglobulin-like domains (D1-3). Deletion experiments of these domains show that D2 and D3 are the FGF binding domains and that heparin binds to a positively charged domain within D2 (Eswarakumar et al. 2005). Crystal structure analysis of FGFR determined that a FGF:FGFR:HSPG complex is needed to produce stable receptor dimerization (Schlessinger et al.2000) as heparin binds to the charged D2 domains on both receptors. Alternate splicing of the immunoglobulin-like domains of FGFR1-3 allows for more ligand specificity as certain FGFs will only bind to certain FGF

receptors. Targeted mutagenesis of FGFRs showed tissue specific expression of the receptors in mice (Eswarakumar et al. 2005). Loss of function (LOF) of FGFR1 and FGFR1-IIIc proved lethal at E9.5 due to defective cell migration through the primitive streak, however LOF of FGFR1-IIIc had no obvious phenotype. FGFR2 and FGFR2-IIIb were also lethal but for different reasons. The FGFR2 lethality was due to a defect in placenta and limb bud formation (E.10.5), whereas FGFR2-IIIb was due to poor development of the lungs and limbs (P0).

Activation and dimerization of FGFR by FGF ligand binding and HSPG complex formation causes transphosphorylation of the intracellular tyrosine kinase domains (Eswarakumar et al. 2005). This provides a docking platform for certain proteins to initiate intracellular signalling pathways. The two main proteins which bind to the activated FGFR are fibroblast growth factor receptor substrate 2 (FRS2) and Phospholipase Cγ (PLCγ) (Figure 1). FRS2 recruits growth factor receptor bound protein 2 (GRB2) which leads to the stimulation of the mitogen activated protein kinase (MAPK) pathway and the PI3K-AKT pathway, resulting in protein transcription changes (Eswarakumar et al. 2005). The MAPK pathway results in mainly proliferative cell signals being activated while the PI3K-AKT pathway causes anti-apoptotic signals, while both contribute to cell migration (Wesche et al., 2011). PLCγ binds to a phosphosite on the c-terminal tail of the FGFR and causes activation of protein kinase C (PKC) (Turner and Grose, 2010). The JAK-STAT pathway is also independently activated by FGFR phosphorylation (Hart et al., 2000).

Src is a tyrosine kinase protein which also binds to FRS2 and has a wide network of downstream substrates such as DOK1, paxillin, FAK1 and EGFR which are involved in a variety of functions from initiating signalling pathways to cytoskeletal attachment to the extracellular membrane (Cunningham et al., 2009). Active Src plays a role in transport of

intracellular FGFR to the plasma membrane requiring RhoB endosomes and assembly of the actin cytoskeleton (Sandilands et al., 2007).

FGF signalling also stimulates several feedback mechanisms to regulate its own activity. Sprouty binds to GRB2 causing negative regulation of downstream signalling however ERK inhibition is not affected by the Sprouty:GRB2 interaction (Martínez et al., 2007). MKP3 and SEF compete for substrate binding and cause receptor dephosphorylation. (Li et al., 2007; Kovalenko et al., 2003). Src activation by FRS2 directly phosphorylates human Sprouty 2 (hSpry2) which is required to reduce signalling of the MAPK pathway via ERK (Li et al. 2004). The E3 ubiquitin ligase Cbl responds to receptor stimulation by causing the ubiquitination and subsequent degradation of FGFR and FRS2 (Wong et al., 2002).

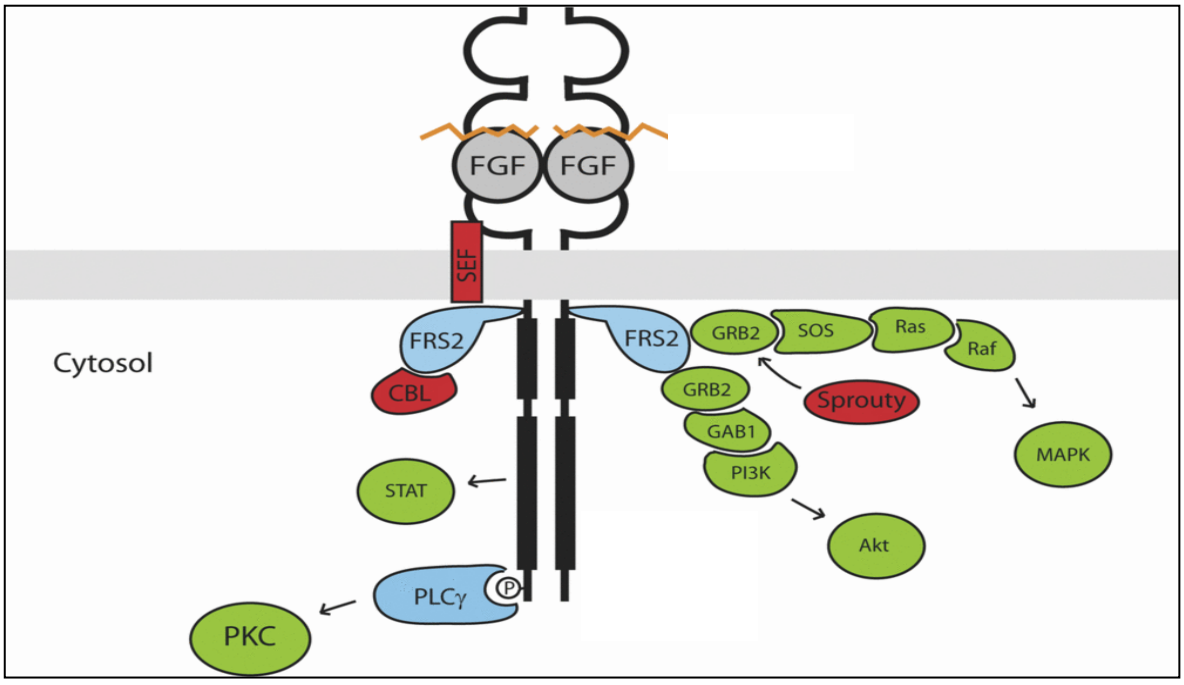

Figure 1 - FGFR Signalling (Adapted from Wesche et al., 2011)
The FGF, heparin, FGFR complex causes dimerization of the receptor and transphosphorylation of the intracellular tyrosine kinase domain. FRS2 binds directly to FGFR and its phosphorylation recruits GRB2 leading to stimulation of the MAPK and PI3K-AKT pathways. PLCγ also binds directly to FGFR and activates PKC. JAK-STAT signalling is also stimulated. Feedback mechanisms Sprouty, SEF and CBL act to attenuate FGFR signalling. Direct FGFR substrates coloured blue, downstream activated proteins coloured green, negative regulators coloured red.

several skeletal disorders (Webster and Donoghue. 1997). There are a number of different FGFR2 mutations seen in craniosynostosis disorders such as Apert, Crouzon, Jackson-Weiss

and Pfeiffer syndromes, with an FGFR1 mutation only seen in Pfeiffer syndrome. Mutations in FGFR3, which is expressed in long bone, is associated with several forms of dwarfism. Around 97% of achondroplasia, the most common form of dwarfism, is due to a glycine to arginine substitution mutation (Gly380Arg).

Aberrant signalling from FGFRs is likely to cause the development and progression of tumours due to their effect on cell proliferation, anti-apoptotic and angiogenesis factors. This aberrant signalling can occur for a number of reasons. As with the skeletal disorders above constitutively activating mutations causing ligand independent promotion of dimerization has been seen repeatedly with FGFR3 in bladder cancer and with FGFR2 in endometrial cancers (Wesche et al., 2011). Mutations in the tyrosine kinase domain of FGFRs can also cause ligand independent constitutive activation. Mutations of the kinase domain of FGFR4 have been identified as potential oncogenes in rhabdomyosarcoma (RMS), a childhood skeletal muscle cancer (Taylor et al., 2009). Constitutive activation of the kinase domain may also occur through the formation of a fusion protein such as the fusion of the kinase domain of FGFR1 to a dimerization domain of a separate protein seen in stem cell leukaemia lymphoma syndrome (SCLL) (Jackson et al., 2009). Single nucleotide polymorphism (SNP) found in FGFRs are also associated with cancers. The SNP G388R found in FGFR4 is thought to confer sustained signalling capabilities compared to wild type and therefore is suggested to contribute to the progression of the several forms of cancer it has been found in (Wesche et al., 2011). SNPs found in FGFR2 causing increased expression of the receptor are also liked with increased risk of breast cancer.

Amplification of the FGFR gene can cause overexpression of the receptor leading to more frequent ligand independent dimerization and therefore signalling.

Roughly 10% of breast cancers contain amplification of the chromosomal region 8p11-12 containing FGFR1 (Gelsi-Boyer et al., 2005). This amplification has been shown to correlate

to overexpression of the receptor and increased downstream signalling (Turner et al., 2010a). Amplification of FGFR2 is seen in a further 1-3% of breast cancers and has been shown to cause ligand independent signalling. Decreasing FGFR2 expression with siRNA or inhibiting with a selective FGFR inhibitor caused the FGFR2 amplified breast cancer cell line MFM223 to have a reduced survival compared to non-amplified cell lines (Turner et al. 2010b). This suggests that the downstream kinase signalling from the amplified FGFR2 was required for the growth and survival of the cells and is a main component of the development and progression of the cancer.

This all indicates how effective FGFRs may be as a therapeutic target in cancer and there are currently several FGFR inhibitors in clinical trials. In particular we are interested in the amplification of FGFR1 and FGFR2 in breast cancers. Therefore understanding the phosphorylation events occurring downstream of FGFR in these cells is important to map out the pathways involved. Gaining knowledge of which pathways are inhibited and which are still active with a particular drug will allow greater specificity when designing combination therapies as well as assisting in predictions of drug resistance. Performing large scale proteomic experiments in order to build up our knowledge of this network allows detection of individual levels of proteins, and in particular activated phosphoproteins, within cells (Mann et al., 2002). These proteomic investigations are possible due to recent advancements in mass spectrometry and the software to analyse the data produced.

Cell Lines

The four cell lines investigated were MCF7, MFM223, SUM52PE and CAL120. The MCF7 cell line was isolated from a 69 year old Caucasian with a breast adenocarcinoma in the

1970s (Soule et al., 1973). It responds to FGF but is not FGFR amplified and so was used as a control cell line. MFM223 was established from a ductal mammary carcinoma (Hackenberg et al., 1991). SUM52PE was established from the pleural effusion of a metastatic breast cancer patient (Ethier et al., 1996). Both MFM223 and SUM52PE are triple negative breast cancer cell lines with amplified FGFR2 (Turner et al. 2010). Triple negative breast cancers do not express estrogen, progesterone or epidermal growth factor receptors. CAL120 was established from the pleural effusion of a 43 year old woman in 1991 and is also a triple negative breast cancer cell line but with amplified FGFR1.

Inhibitors

In order to collect information about the phosphorylation network associated with FGFR signalling and to see how certain drugs may affect it, inhibitors of FGFR and Src were chosen. FGFR inhibition will allow us to see what proteins are affected by FGFR signalling and what pathways are still activated and potentially contributing to the progression of the cancer. Src inhibition is also interesting due to its downstream activation following FGFR signalling as well as its role activating and regulating other pathways and its feedback role on the transport of FGFR itself. Initially SU5402, a specific FGFR tyrosine kinase inhibitor, and Dasatinib (a.k.a. Sprycel), a Src family tyrosine kinase inhibitor, which is already in use as a treatment for chronic myeloid leukaemia (CML), were utilised. Further experiments were performed using PD173074 an ATP competitive inhibitor of FGFR and VEGFR as well as Saracatinib a dual specific inhibitor of Src and Abl.

SILAC

Stable Isotope Labelling by Amino Acids in Cell Culture (SILAC) involves the incorporation of heavy atom isotopes into proteins in order for mass spectrometry (MS) proteomic analysis

of the cell (Mann, 2006). Cells are grown in different media containing an amino acid labelled with a stable isotope of a specific atom i.e. deuterium (^{2}H), ^{13}C or ^{15}N. This makes the amino acid (arginine or lysine in this case) slightly heavier than normal. As the cells grow, divide and make new proteins the amino acids in the media are incorporated into the proteins of the cell. Eventually after five cell doublings enough protein synthesis has occurred for all the arginine and lysine amino acids in all the proteins in all the cells to be labelled. Therefore one set of conditions can be performed on the unlabelled set of cells (usually a control) and another set of conditions on the heavier labelled cells. The weight difference produced by the labelling is small enough not to exert a biological effect but large enough to be detected by the mass spectrometer. A big advantage of this technique is that the unlabelled and labelled cells can be mixed together and undergo the digestion, purification, and phosphoenrichment steps as one sample to produce the peptides for analysis. This removes errors which can be produced when dealing with separate samples of cells such as small differences in the amount of solutions applied or the amount of cells lost at each stage. The mass spectra produced from the sample shows each peptide as a pair, one from the unlabelled cells and one a few Da heavier from the labelled cells. Measuring the ratio of intensity between the two peaks gives a direct indication of the amount of peptide in each. A one-to-one ratio shows that there is no difference in abundance of the peptide between the two sets but a statistically significant high or low ratio indicates that the conditions the cells were under caused a change in that peptide's level of abundance within the cell (Mann, 2006).

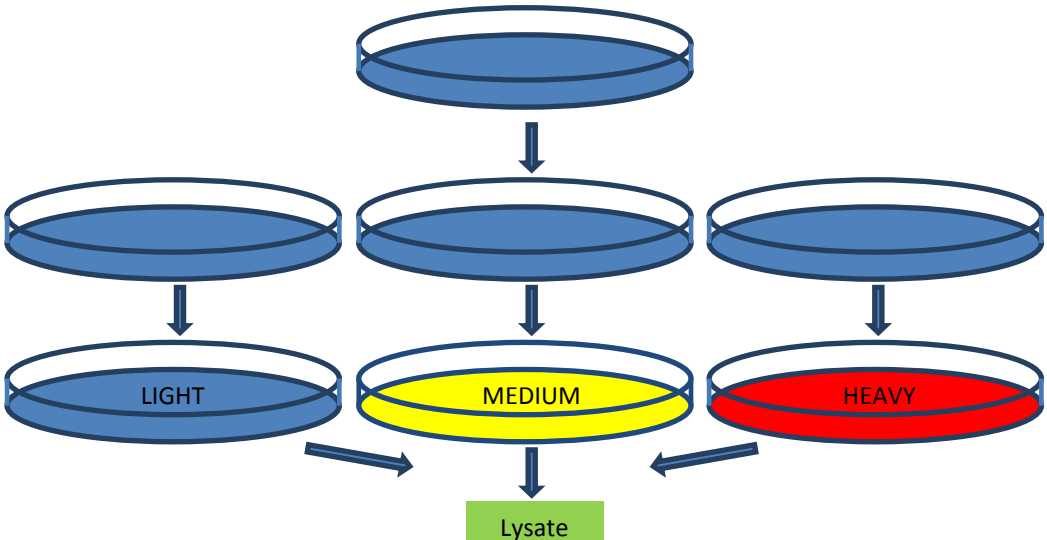

Figure 2 - SILAC Workflow
Cells are split into different populations and grown in light, medium or heavy media. Cell lysate is collected and pooled and proteins digested into peptides with trypsin. A strong cation exchange column can then be used to fractionate the mixture and a further phosphor-enrichment step to purify out phosphorylated peptides. The sample can then undergo mass spectrometry analysis.

Whole cell lysate from the SILAC samples needs to be prepared before undergoing MS analysis. A trypsin digest needs to be performed to break up the proteins into peptide fragments. It is easier to analyse peptide fragments with the MS than whole proteins as the MS is more sensitive to peptides and is most efficient when sequencing chains of up to 20 amino acids. Proteins are also more difficult to handle and can have problems with solubility and interactions with other proteins in comparison to peptides (Steen and Mann. 2004). Trypsin always cleaves at the arginine or lysine from the C-terminal (Olsen et al. 2004) and so the peptides produced can be predicted. Desalting the sample to remove impurities that would damage the MS equipment and produce meaningless results needs to occur. This is done using a process whereby the lysate is passed through a trap where proteins bind and are unable to flow through. Then using usually a high acidic solution the peptides can be eluted back off and collected.

If the sample is highly concentrated and contains a complex mixture of peptides it is advisable to fractionate it into smaller sections. This prevents overloading of the MS and

allows less abundant peptides a greater chance of detection. Putting the sample through a strong cation exchange column where the charged peptides are attracted to the column and are eluted over time by an increasing salt gradient is one way of doing this.

The same trapping and eluting process can also be used to extract the phosphorylated peptides out of the sample. Titanium dioxide (TiO_2) beads in a specialised pipette tip can be used to bind the phosphopeptides with an ammonium hydroxide/pyrrolidine solution applied to elute. Further desalting then allows the sample to reach MS analysis quality.

To enter the MS the sample is loaded into a high performance liquid chromatography (HPLC) column which elutes the peptides into the MS over time, based on an increasing acetonitrile gradient which removes peptides in order of their hydrophobicity. As peptides enter the Orbitrap Velos MS as a liquid they are vaporised and subsequently ionised in a process of electrospray ionization. The ionised peptides are then trapped in an electric field and released onto the detector sequentially depending on their mass to charge ratio (m/z) (Steen and Mann, 2004). This provides information on the mass and intensity of each peptide but this doesn't give enough information to determine the peptide sequence or which protein it came from. The MS is able to accomplish this by taking a peptide ion and fragmenting it by colliding it with inert helium gas atoms. This produces a predictable set of peptide fragments on which MS can be performed again. The resulting spectra should show each peptide fragment in a sequence, with one amino acid difference. That amino acid can be determined by the mass difference between the peaks and as there are only a finite number of amino acid combinations that actually occur it is relatively simple for algorithm software such as Sequest or Mascot to search known peptide databases and accomplish this. When the peptide sequence is known it can be searched against a protein database to determine where it came from. (Steen and Mann, 2004)

MaxQuant is the software which uses several algorithms to calculate from the mass spectra the quantitative proteomics of the SILAC experiment. It uses an integrated Andromeda search engine to produce the peptide sequences (Cox et al., 2011) from which it is able to produce the ratios between the peptides containing the heavy, medium and light amino acids. It does this by fitting a Gaussian peak over three data points for each peak it finds. It then uses the subsequent mass spectra at that point to build up a 3D plot of the m/z-retention over time. Peaks that are different by a mass equal to the mass of the labels and show correlation between their 3d plots are SILAC pairs, i.e. the same peptide but labelled differently. The intensity of the peaks can then be compared to give a ratio (Cox and Mann. 2008).

Aims

Certain breast cancers are characterised by amplification of FGFRs whose activation is likely to cause proliferation of cells and progression of the cancer. Understanding the phosphorylation signalling events occurring downstream when FGFRs are activated by detecting how certain drugs are able to inhibit this process will help produce a molecular profile of specific breast cancers. Obtaining this profile will hopefully lead to the possibility of quicker, more detailed prognosis and more specialised treatment for patients with amplified FGFR breast cancer cells. We looked at four breast cancer cell lines and the effect that inhibitors of FGFR and Src had on FGFR signalling by using specific antibody staining and whole cell proteomics.

Materials and Methods

Cell Culture

MCF7, CAL120 and MFM223 cell lines were grown at 37^{o}C, 5% CO_2 in DMEM cell media containing 2mM L-Glutamine (Lonza) supplemented with 10% Foetal Bovine Serum (FBS) and antibiotics (Penicillin 0.2 U/ml and Streptomycin 0.1mg/ml). SUM52PE cells were grown as above but substituting DMEM for RPMI. Cells were grown in 75cm^2 cell culture flasks with 15ml media and split twice a week (MCF7, CAL120, SUM52PE usually 1:4 or 1:5. MFM223 usually 1:3). A 5 minute incubation with 1ml of 0.05% Trypsin-EDTA (1X), Phenol Red was used to detach the cells from the surface of the flask when splitting.

Cell Treatment and Lysis

Cells were split into 6-well plates containing 3ml media prior to treatment and allowed to adhere and reach a confluencey of ~70%. Cells were then serum starved in 2ml media (no FBS) for 4 hours. For those cells requiring inhibitor treatment, inhibitors were added 30 minutes prior to any growth factor stimulation. For those cells requiring FGF stimulation, heparin (10ug/ml) and FGF1 (20ng/ml) were added and cells were incubated for 30 minutes. Cells were then washed twice in 1ml ice cold PBS and then lysis buffer, made up of 50mM Tris/HCL, 1% TX-100, 150mM NaCl, with 1 Roche PhosSTOP tablet and 1 Roche Mini-Complete Protease tablet added to 10ml of buffer prior to use, (65-100µl depending on the final concentration of protein required) was added and left on ice or at 4^{o}C for 30 minutes. Cells were scraped from the bottom of the wells and centrifuged at 13,000 rpm for 20 minutes (4^{o}C). Supernatant was collected as whole cell lysate and frozen at -70^{o}C for later use.

Protein Concentration Calculation (Bradford Assay)

Using a 96 well plate, standards ranging from 2000µg/ml to 25µg/ml were added in duplicate (5µl per well). Samples were diluted to x5 and x10 and placed in triplicate in wells (5µl each). Coomassie Plus protein assay reagent (250µl) was added to each well. An Emax precision microplate reader was used to detect the optical density at 590nm wavelength. SOFTmax software was used to analyse the data and plot a standard curve from which the absorbance readings of the unknown samples were converted into protein concentrations.

SDS-PAGE

Whole cell lysate samples were diluted to equivalent concentrations in lysis buffer prior to the addition of Reducing Sample Buffer (RSB) x4 and Sample Reducing Agent (DTT) x10. Usually 20µl of sample was added to each well of a NuPAGE 4-12% Bis-Tris gel prior to running in MOPS SDS Running Buffer at an initial voltage of 120V, increasing to 200V after 10 minutes. PageRuler Prestained Protein Ladder marker (3µl) was run alongside the whole cell lysate samples.

Western Blotting

PVDF membrane was soaked in methanol for 5 minutes. Transfer buffer consisted of methanol (10%), 12mM Tris and 96mM Glycine. Transfer from gel to PVDF membrane was performed at 4^{o}C, at 100V for 1 hour 15 minutes. The membrane was blocked in methanol after transfer for 2 minutes and allowed to air dry. Primary antibodies were diluted in a solution of 50% PBS, 50% Odyssey Blocking Buffer, 0.1% Tween (8-10ml total) normally in a 1:1000 ratio. They were then added to the membrane which was rocked in an opaque box for 1 hour at room temperature or overnight at 4^{o}C. Membranes were washed in PBS, 0.1% Tween (PBS-T) four times for at least 10 minutes each. Mouse or rabbit secondary antibody, labelled with fluorophores emitting at a 680 or 800nm wavelength, was diluted in a 1:15000

ratio in 50% PBS, 50% Odyssey Blocking Buffer, 0.1% Tween, 0.01% SDS (10ml total). Membranes were rocked for 1 hour at room temperature then washed 4 times in PBS-T for at least 10 minutes each time. Membranes were washed in PBS for 10 minutes and fresh PBS applied before detecting with a LI-COR Odyssey Elite infrared scanner.

Primary Antibodies – **p653/654** (Mouse; Y-653/654; Cell Signaling Technology), **Bek** (Rabbit; C-17; Santa Cruz Biotechnology), **Flg** (Rabbit; C-15; Santa Cruz Biotechnology), **p-ERK** (Mouse; Y-204; Santa Cruz Biotechnology), **ERK** (Rabbit; K-23; Santa Cruz Biotechnology), **p-Src** (Rabbit; Y-416; Cell Signaling Technology), **Src** (Mouse; L4A1; Cell Signaling Technology), **p-AKT** (Rabbit; T308, Cell Signaling Technology), **AKT** (Mouse; 40D4; Cell Signaling Technology).

SILAC

CAL120 cells were grown separately in amino acid deficient DMEM media supplemented with isotopically distinct arginine and lysine. The heavy media contained added arginine(R) +10Da and lysine(K) +8Da, the medium media contained R +6Da and K +4Da and the light media contained isotopically normal R and K, all at 0.1mg/ml. Cells were grown for at least five doubling times prior to use. Labelled cells were plated in three 15cm dishes containing 25ml media. Following serum starvation in 20ml media inhibition and FGF stimulation treatment the whole cell lysate was collected as described previously. A total of 800µl lysis buffer was used to lyse cells in each dish.

Trypsin Digestion – In Solution

A mixture of 5mg protein from each sample was collected. A trypsin digest was performed by incubating overnight at 37^0C with Promega Trypsin Gold 1µg/µl stock, in a 1:100 ratio to the sample. The digested sample was desalted using SEP-PAK Plus Light cartridges by being

loaded in 0.4% TFA, desalted/washed with 0.1% TFA, then 0.5% acetic acid (HAcO) and finally eluted with 50% acetonitrile (ACN), 0.5% HAcO.

-In Gel

Bands of the gel containing desired proteins were excised and diced into small pieces. These were dehydrated in a vacuum centrifuge for 5 minutes (no heat) and then rehydrated in 10mM DTT, 25mM ammonium bicarbonate at 56^0C for 45 minutes. This was replaced with 55mM iodoacetamide, 25mM ammonium bicarbonate at room temperature for 45 minutes to alkylate and then washed with 25mM ammonium bicarbonate (1 x 10 minutes) and 50% ACN, 25mM ammonium bicarbonate (2 x 5 minutes). The gel pieces were then dehydrated again (5 minutes, no heat) and rehydrated for 10 minutes in a 12.5 ng/µl trypsin solution (50mM acetic acid, 25mM ammonium bicarbonate). Excess was removed and pieces covered in 25mM ammonium bicarbonate overnight at 37^0C before formic acid was added to a final concentration of 0.5% and solution removed. Finally 2 x 50% ACN and 1 x 100% ACN were added with vigorous agitation to extract any remaining peptides. Supernatants were pooled to collect all extracted peptides.

Strong Cation Exchange

The sample was run through a 100x 4.6mm Polysulfoethyl Aspartamide strong cation exchange (SCX) column (5µm particle size, 200Å pore size), with 'javelin' type guard, to fractionate. Mobile phase A was a 10mM KH_2PO_4, 20% ACN (pH3 acidified by phosphoric acid) solution and mobile phase B was the same with 500mM KCl. The column was equilibrated for 5 minutes with mobile phase A and a gradient of 0-30% mobile phase B was

added over 30 minutes which increased to 50% over 5 minutes and returned to 0% for 20 minutes at a flow rate of around 1ml/min. Fractions were combined to produce 20 samples which were desalted and concentrated using a MacroTrap by loading samples in 2% ACN, 0.1% TFA, then desalting with the same and eluting with 70% or 90% ACN.

Phosphoenrichment

Samples were phosphoenriched with a Titansphere Phos-TiO Spin Tip Kit and eluted using 5% ammonium hydroxide and 5% pyrrolidine. Samples were finally desalted again using Zip Tips, loading with 0.1% TFA and eluting with 0.1% formic acid, 50% ACN.

Liquid Chromatography

Peptides were loaded onto a 150mm Acclaim PepMap100 C18 column (LC Packings, Sunnyvale, CA) in mobile phase A (0.1% formic acid. JT Baker, Holland. Sigma Aldrich). Peptides were separated from the column over a linear gradient of 3.2% to 44% mobile phase B (ACN + 0.1% formic acid. JT Baker, Sigma) at a flow rate of 350 nl/min. The column oven was heated to 35^0C. For standard (non-FAIMS) LC-MS/MS the LC system was coupled to an Advion Triversa Nanomate (Advion, Ithaca, NY) which infused the peptides with a spray voltage of 1.7 kV. Peptides were infused directly into the LTQ-Orbitrap Velos ETD (Thermo Fischer Scientific, Bremen, Germany).

Tandem Mass Spectrometry (MS/MS)

Collision induced dissociation (CID) MS/MS scans of the seven most abundant ions above a threshold of 1,000 were taken. Survey scans were acquired in the Orbitrap with a resolution of 60,000 at *m/z* 400. The seven most abundant multiply charged precursor ions were subjected to CID in the linear ion trap. The idth of the precursor isolation window was 2 *m/z*

and only multiply charged precursor ions were subjected to CID. CID was performed with helium gas at a normalized collision energy of 35% (target 5 $x10^4$, maximum fill time 100 ms). CID activation was performed for 10 ms. Dynamic exclusion repeat count was set to 1 with duration of 60 s. Data acquisition was controlled by Xcalibur 2.1 (Thermo Fisher Scientific).

MaxQuant

Version 1.3.0.5 with integrated Andromeda search engine was used and data was searched against the human Swiss-Prot database (updated Jan 9th 2013). The parameters selected to search against were with a protease of trypsin and variable modifications of oxidation, acetylation and phosphorylation. The labels searched for were arginine +6Da; lysine +4Da and arginine +10Da; lysine +8Da. Maximum missed cleavages was set at two and a false discovery rate of 1% was incorporated into the search.

Results

Firstly we detected if amplification of the FGFR genes in each cell line related to over expression of the active protein (Figure 3). SUM52 and MFM223 the FGFR2 amplified cell lines showed a large expression of the active phosphorylated receptor with and without FGF stimulation. There is an indication of CAL120 active FGFR1 overexpression but it is not totally clear from this western. FGF stimulation increased active receptor number in the three amplified breast cancer cell lines but did not seem to have a significant difference in MCF7 cells.

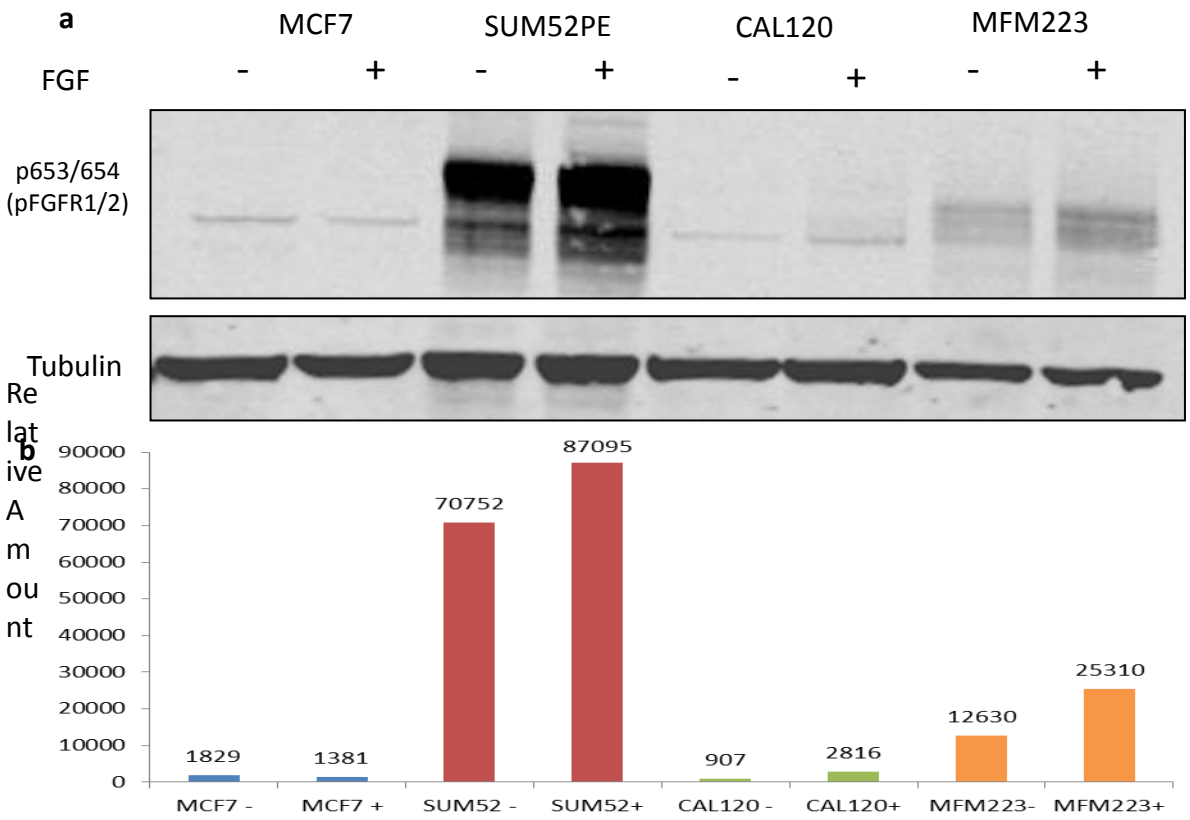

Figure 3 – Active FGFR Receptor Levels in Cell Lines
A – Western blots of phosphorylated FGFR1 and FGFR2 using p653/654 antibody in each cell line with and without stimulation via FGF1 (20ng/ml). Tubulin blot used as a loading control. B – Quantification of western blots.

SU5402 and Dasatinib Effect on Cell Signalling

Initially each cell line was treated with SU5402 a FGFR inhibitor (Mohammadi et al., 1997) and Dasatinib a Src inhibitor (Lombardo et al., 2004) in order to test their function as inhibitors of FGFR and Src respectively. The concentrations used were 20μM SU5402 and 20nM Dasatinib. These concentrations had previously been shown to produce effective inhibition in titration experiments in HEK293T cells and were therefore designated as ideal concentrations to use in a SILAC experiment. Each cell line was plated into 4 wells and then serum starved to reduce any ligand dependent signalling present in the cells. One well then received the 20μM SU5402 and another 20nM Dasatinib. After a half an hour equilibration the cells, to which the inhibitors had been added and one to which they had not, were stimulated by addition of 20ng/ml FGF1 as well as an excess of heparin (10ug/ml) to assist receptor activation. Another half an hour incubation allowed enough time for downstream signalling events to occur (Cunningham et al., 2010). Cell signalling was halted by addition of ice cold PBS, the reduction in temperature of the cells preventing further changes in phosphorylation. Whole cell lysate from each cell line was collected and protein concentration was measured. This was done in order to try and load the same amount of sample in each column of the gel, so higher concentration lysates were diluted to the same concentration as the lowest concentration lysate of the cell line. Sodium dodecyl sulphate polyacrylamide gel electrophoresis (SDS-PAGE) was used to separate proteins in the lysate according to their molecular weight. After being run the gel and transferred to a membrane. Western blots were performed looking for FGFR1, FGFR2, ERK and Src as well as active phosphorylated versions using primary antibodies to detect the protein and secondary antibodies labelled with a fluorophore to detect the primary antibody. The antibody to detect phosphorylated FGFR bind when tyrosines 653/654 are phosphorylated.

The western blots show SU5402 at 20μM clearly inhibits receptor activation in CAL120, SUM52PE and MFM223 cell lines (Figure 4a) and the quantification (Figure 4b) backs this

up showing almost complete loss. It also resulted in a reduction of active ERK (p-ERK). Active Src levels (p-Src) were not affected though.

Dasatinib did not show any inhibition of the receptor or ERK at this concentration, but did inhibit Src (Figure 4c). As the levels of p-Src were very low in the cells the amount of antibody used was increased to a 1:800 ratio. However either due to the increase in antibody or too much sample loaded the resulting blurred bands made quantification of the effectiveness of the drug difficult to be certain about.

Comparison of ligand independent activation to FGF stimulated activation show that SUM52PE FGFR1/2 activation was only slightly increased, MFM223 was more than doubled whereas CAL120 was massively increased almost 20 fold. CAL120 FGFR1/2 activation was still higher than ligand independent activation when SU5402 inhibition was used.

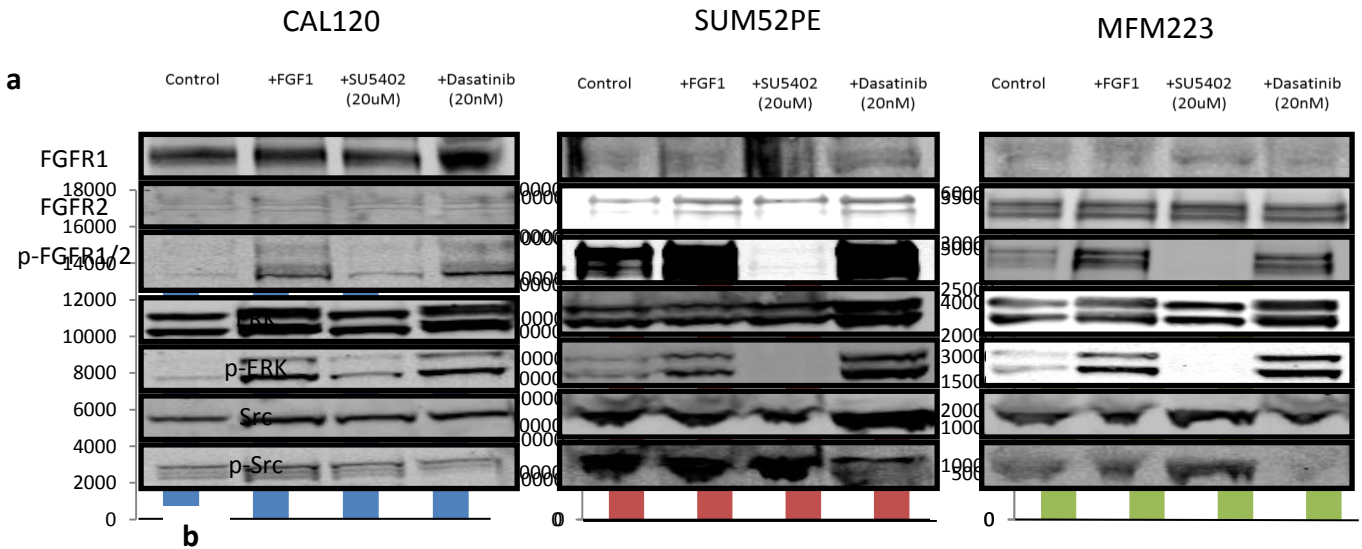

Phosphoenrichment Method Development

The phosphoenrichment stage of the SILAC method, as explained before, is important to allow detection of the phosphoproteome. The method involves loading the sample into a Phos-TiO_2 Spin Tip in which phosphopeptides are retained as the phosphate groups form bonds with the titanium dioxide under acidic conditions, and non-phosphopeptides flow through as waste. Then an alkaline elution solution is passed through to remove the phosphopeptides from the tip, allowing collection of the enriched sample to run on the MS. Previous experiments in the lab using an elution solution of 1.75% ammonium hydroxide resulted in relatively low numbers of phosphopeptides being detected at the MS stage. This suggested that a number of the phosphopeptides were being retained in the spin tip and that the method of elution was not effective enough. A change in protocol to using a 5% ammonium hydroxide and then a 5% pyrollidine solution to elute with was suggested by the manufacturer (GL Sciences Inc.) to be more effective as it is more basic and was thought to cause elution of different peptides. To test this a sample containing eight synthetic phosphopeptides was split and underwent Phos-TiO_2 Spin Tip phosphoenrichment, one being eluted with1.75% ammonium hydroxide solution and the other eluted with5% ammonium hydroxide and a 5% pyrollidine solution. The samples were then desalted using ZipTips and run through the MS. The spectra produced were searched manually for the peptides as the sequence and therefore molecular mass of each peptide was known. The intensity of each peptide was identified and compared to the intensity produced with each method of elution (Figure 5a). There was an increase in intensity of all eight phosphopeptides, with a greater recovery for some compared to others.

a

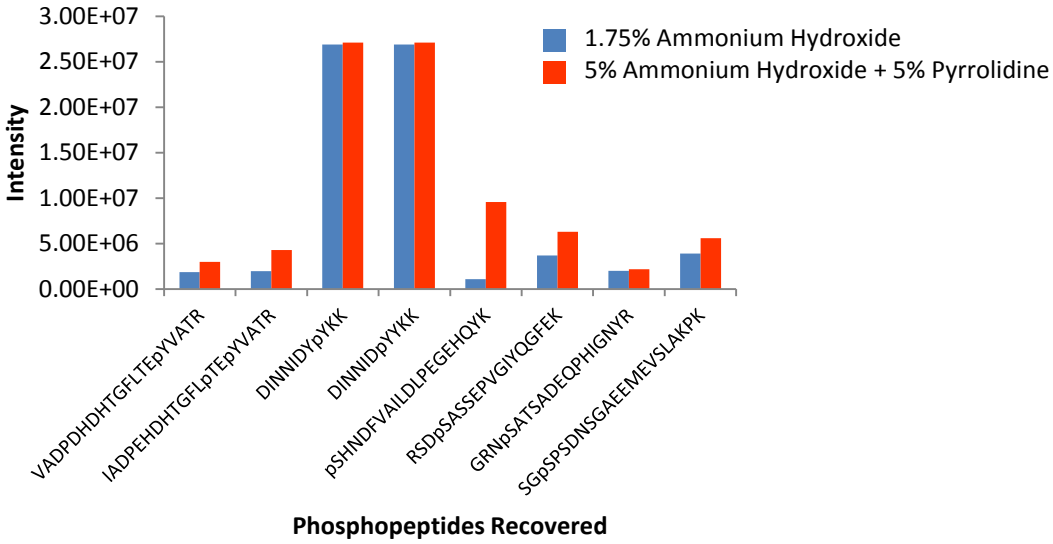

b

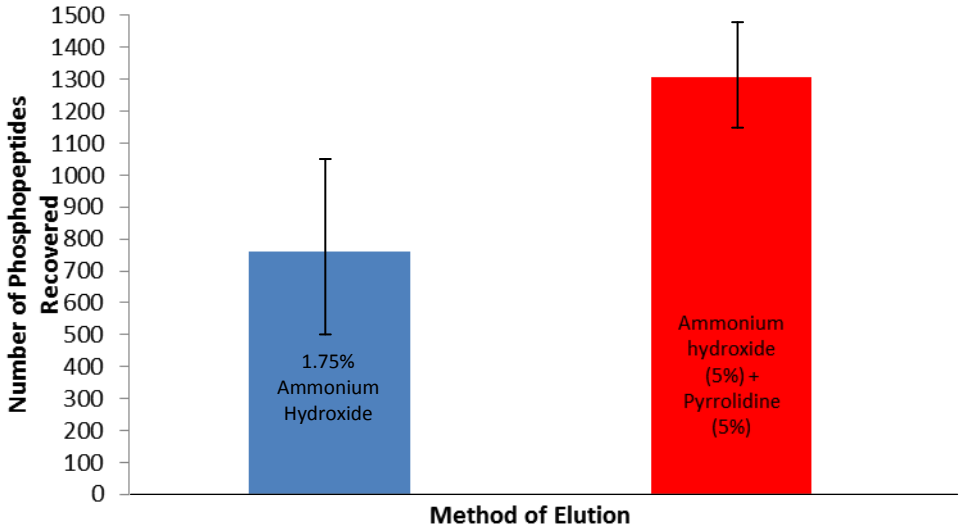

Figure 5 – Phosphoenrichment Method Development
Testing method of elution during Phos-TiO_2 Spin Tip phosphoenrichment between the 1.75% ammonium hydroxide solution or the 5% ammonium hydroxide plus 5% pyrrolidine solution. Phosphopeptide amounts measured using MS. A – Intensity of eight known phosphopeptides recovered by either method. B – number of phosphopeptides recovered by either method from a MFM223 whole cell lysate sample. (n=2).

This proves that the 5% ammonium hydroxide/ 5% pyrollidine method is able to remove more of these peptides but a more complex sample was needed to test if the method could elute a wider range of phosphopeptides as well. A sample of MFM223 whole cell lysate was used to provide a more complex mixture of phosphoproteins. The sample was desalted with a Macrotrap before performing Phos-TiO_2 Spin Tip phosphoenrichment with both methods in

duplicate. Samples were then desalted with ZipTips and run on the MS. The spectra produced were searched using the Mascot and SEQUEST algorithms against a database of possible peptide sequences. A list of peptides was produced from which the number of phosphopeptides recovered via each method could be identified (Figure 5b). The 5% ammonium hydroxide/ 5% pyrollidine method recovered on average over a third more individual phosphopeptides. Therefore using a 5% ammonium hydroxide and then a 5% pyrollidine solution is a far more effective method of elution and, as it doesn't take any longer to complete than the 1.75% ammonium hydroxide method, is now standard protocol.

CAL120 SILAC Using SU5402 and Dasatinib

CAL120s were chosen as the cell line for the SILAC experiment as their reported FGFR1 amplification suggested that an interesting response would be produced. Also killing curve data looking at CAL120s over several days following SU5402 or Dasatinib inhibition found that CAL120s showed a ~50% survival rate, suggesting that they are not totally reliant on FGFR or Src signalling for growth and survival (Cunningham. 2012, unpublished). Detection of pathways still active or upregulated when inhibitors are added may indicate reasons for the cell survival. Cells were grown to a large volume to produce a suitable amount of protein for the MS analysis. The cells grown in medium labelled media were treated with 20μM SU5402. Cells grown in the heavy labelled media were treated with 1μM Dasatinib. This is a large increase from the amount tested previously but was chosen as the effectiveness of the 20nM concentration was not conclusively proven and substantial inhibition was required. Dasatinib at 1μM is the highest concentration detected in plasma following treatment of CML. Inhibitors were added 30 minutes before FGF1 and heparin stimulation and whole cell lysate collected as previously described. Protein amount was calculated and 5mg of protein from each labelling was added together for the trypsin digest. The sample was desalted twice with Sep-Pak as it was too concentrated initially for the cartridges to hold all the peptides. The sample was then run through the SCX which split it into 50 fractions (Figure 6a). These were combined into 20 samples, each containing less than 10% of the total amount of peptides. The samples were then desalted using a MacroTrap and a higher elution solution of 90% ACN, compared to the 70% used when preparing the method development samples, in order to ensure all peptides came off the trap. Phosphoenrichment was performed using the 5% ammonium hydroxide/5% pyrollidine elution method and final desalting with ZipTips produced MS ready samples. Sample volume was decreased at the stages requiring it by a centrifugal evaporator (SpeedVac).

a

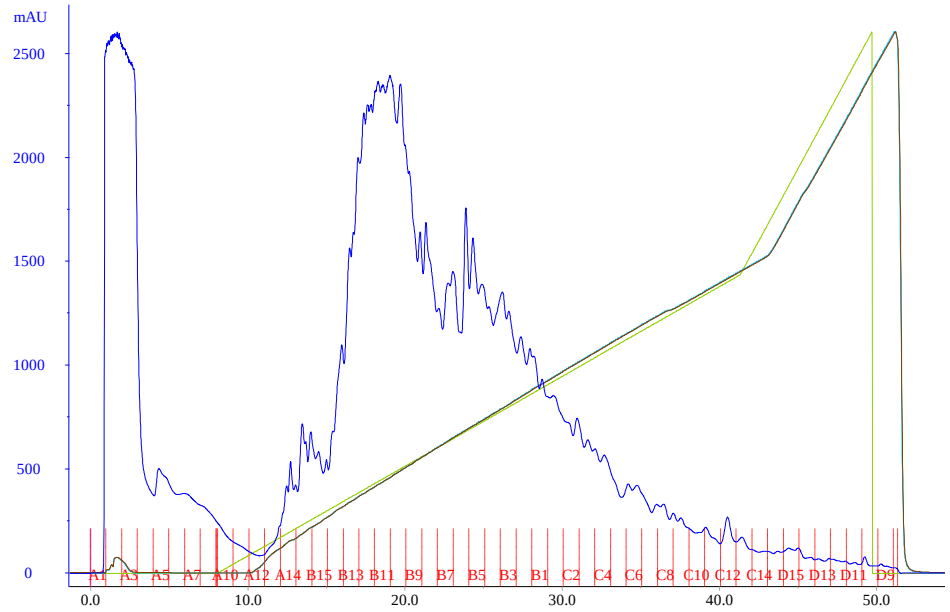

Sample	1	2	3	4	5	6+7	8+9	10+11	12	13	14	15	16	17	18	19	20
Fraction	A2-A4	A5–A13	A14-B15	B14	B13	B12	B11	B10	B9	B8	B7	B6	B5	B4	B3,B2	B1-C3	C4–End

b

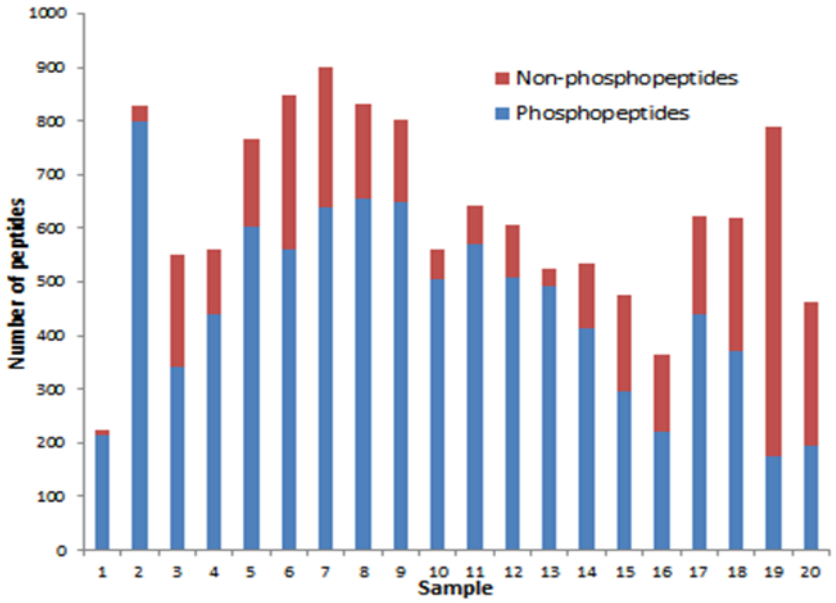

Figure 6 – Strong Cation Exchange Fractionation

A - Trace of the fractionation of peptide mixture when put through a strong cation exchange column. Blue line represents concentration of peptides being released over time. Red columns indicate fractions. Table shows which fractions were combined to form the 20 samples to run on the mass spectrometer. B - numbers of phosphopeptides and non-phosphopeptides identified from each sample when run on the MS.

the peptides present. Ratios between intensities found in the uninhibited light cells (L),

SU5402 inhibited medium cells (M) and Dasatinib inhibited heavy cells (H) were given but because of the phosphoenrichment and inhibition of many of the phosphopeptides it skewed the normalisation calculated by the software as a lot of the peptides coming from the different cells were likely to be found in differing quantities. To correct this a sample of cell lysate mixture from each of the labelled cells containing the same amount of protein was run on a gel column. Two bands were cut out and the proteins removed and broken up by an in gel trypsin digest. The peptides were then run on the MS and analysed by MaxQuant, producing a list containing mainly non-phosphorylated peptides. These provided a much better comparison between the labelled populations and provided the correction value needed to be added to the initial data to normalise it properly. The gel slice data also provided the normal distribution from which cut off values of significantly higher and lower ratios (> 1.73 or < 0.58), taken at two standard deviations from the mean, could be calculated. This provided a 95% certainty that the ratio was different due to the conditions applied and not just random variation. The phosphoenriched data set was then normalised and had reverse hits, which are the same peptide but sequenced backwards, and obvious contaminants such as non-human proteins, removed. Some of the peptides labelled as contaminants in the data set such as keratin are actually present in cells so were left in. However they could still be identified as a contaminant if the ratios showed that there was no labelled version of the peptide, indicating that it must have come from an outside source. The ratios produced were medium to light (M/L) which compared the peptides found in the SU5402 treated cells to the untreated light cells. The heavy to light (H/L) comparing Dasatinib treated and untreated cells and finally heavy to medium (H/M) comparing Dasatinib to SU5402 treated cells. A ratio of 1 would indicate that the levels of peptide were the same and no change had occurred. A ratio lower or higher than the statistically significant cut off points indicated that that peptide had been changed by the inhibitor treatment.

Plotting $\log_2$ of the M/L and H/L ratios shows the spread of the data (Figure 7a). Of the ~12500 individual peptides found almost 10% were decreased or increased in the amount detected with addition of either inhibitor. Many were only decreased with addition of one of the inhibitors and not the other indicating the differing methods of action and effects of the drugs. Several peptides were increased by the addition of the inhibitors which may indicate changes in regulatory components or compensatory pathway activation necessary for the continued growth and survival of the cells. Of the peptides identified 72.6% were phosphopeptides and 27.4 were non-phosphopeptides (Figure 6b).

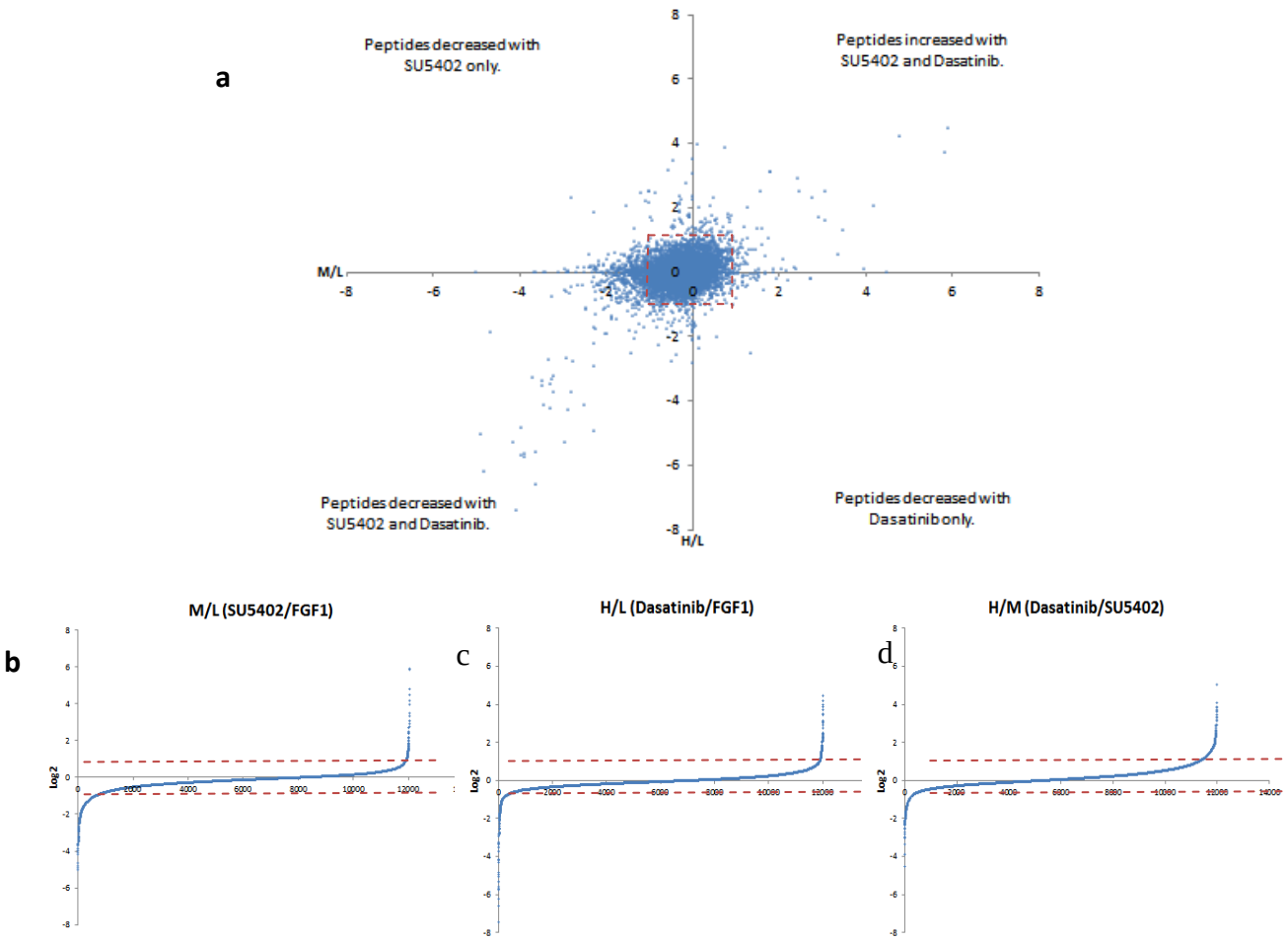

Figure 7 – CAL120 SILAC Data Distribution
A – Scatter plot of the peptides discovered by MS, with $\log_2$ M/L (SU5402/FGF1) ratio plotted against $\log_2$ H/L (Dasatinib/FGF1) ratio. Each blue dot represents one of the 12513 individual peptides. Peptides in the bottom left corner were decreased with both SU5402 and Dasatinib. Peptides in the top left corner were decreased with SU5402 only. Peptides in the bottom right corner were decreased with Dasatinib only. Peptides in the top right corner were increased with SU5402 and Dasatinib. B – Plot of log2 M/L (SU5402/FGF1) ratio against peptide number. C - Plot of log2 H/L (Dasatinib/FGF1) ratio against peptide number. D - Plot of log2 H/M (Dasatinib/SU5402) ratio against peptide number. (Dashed red line indicates cut off points for statistically higher or lower amounts of peptide).

Applying the cut off values to the data set showed that out of a total of 9087 phosphopeptides recovered, 995 and 249 were lower when SU5402 and Dasatinib were used respectively (Figure 8a). This was condensed to 340 proteins having a reduced level of phosphorylation at a specific site when SU5402 was added and 131 proteins with Dasatinib, with 73 of those proteins being the same (Figure 8b). A total of 154 phosphopeptides relating to 90 proteins

became higher with addition of SU5402 while 221 phosphopeptides and 128 proteins were higher with Dasatinib.

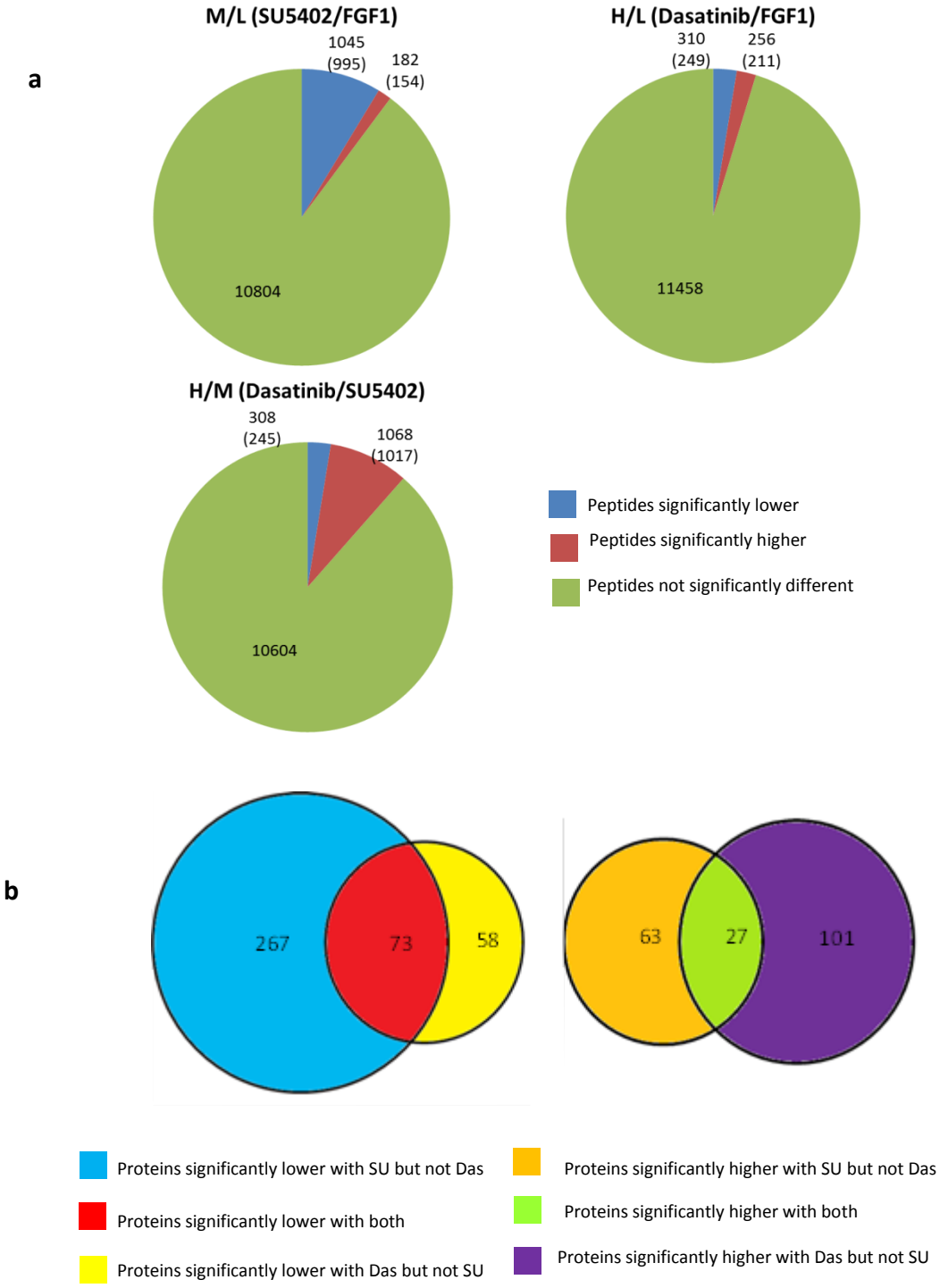

Figure 8 – CAL120 SILAC Experiment Data Analysis
A – Pie charts showing numbers of peptides from each ratio comparison which are significantly higher or lower. Numbers of phosphopeptides are in brackets. B – Venn diagrams showing the numbers of phospho-proteins which are significantly changed by inhibitor addition.

The proteins with significantly decreased levels of phosphorylation at a specific phosphosite were then analysed for any pathways or functional groups which could be identified. STRING (Search Tool for the Retrieval of Interacting Genes/Proteins) is a database used to identify protein-protein interactions based on evidence from experiments and previous database knowledge. The map produced when phospho-proteins significantly lower with SU5402 showed two clear clusters of interaction (Figure 9a). Functional analysis of proteins in the smaller cluster identified several which play a role in RNA processing and transport. The larger cluster contains many proteins involved in the MAPK pathway such as FRS2, son of sevenless (SOS), Raf, mitogen-activated protein kinase 3 (ERK1) and mitogen-activated protein kinase 1 (ERK2) (Figure 9b). Many other interesting proteins such as retinoblastoma (Rb), insulin receptor substrate 2 (IRS2) and several serine threonine protein kinases also showed decreased phosphorylation but without any obvious direct interactions or functional grouping.

Proteins found with significantly reduced phosphorylation following treatment with the Src inhibitor Dasatinib had no clear association with signalling pathways downstream of FGFR or in fact with most known Src substrates. Functional analysis with PANTHER (Protein Analysis Through Evolutionary Relationships) found that 14 proteins which were lower were associated with the cytoskeleton such as paxillin, dystonin and several microtubule associated proteins (Table 1).

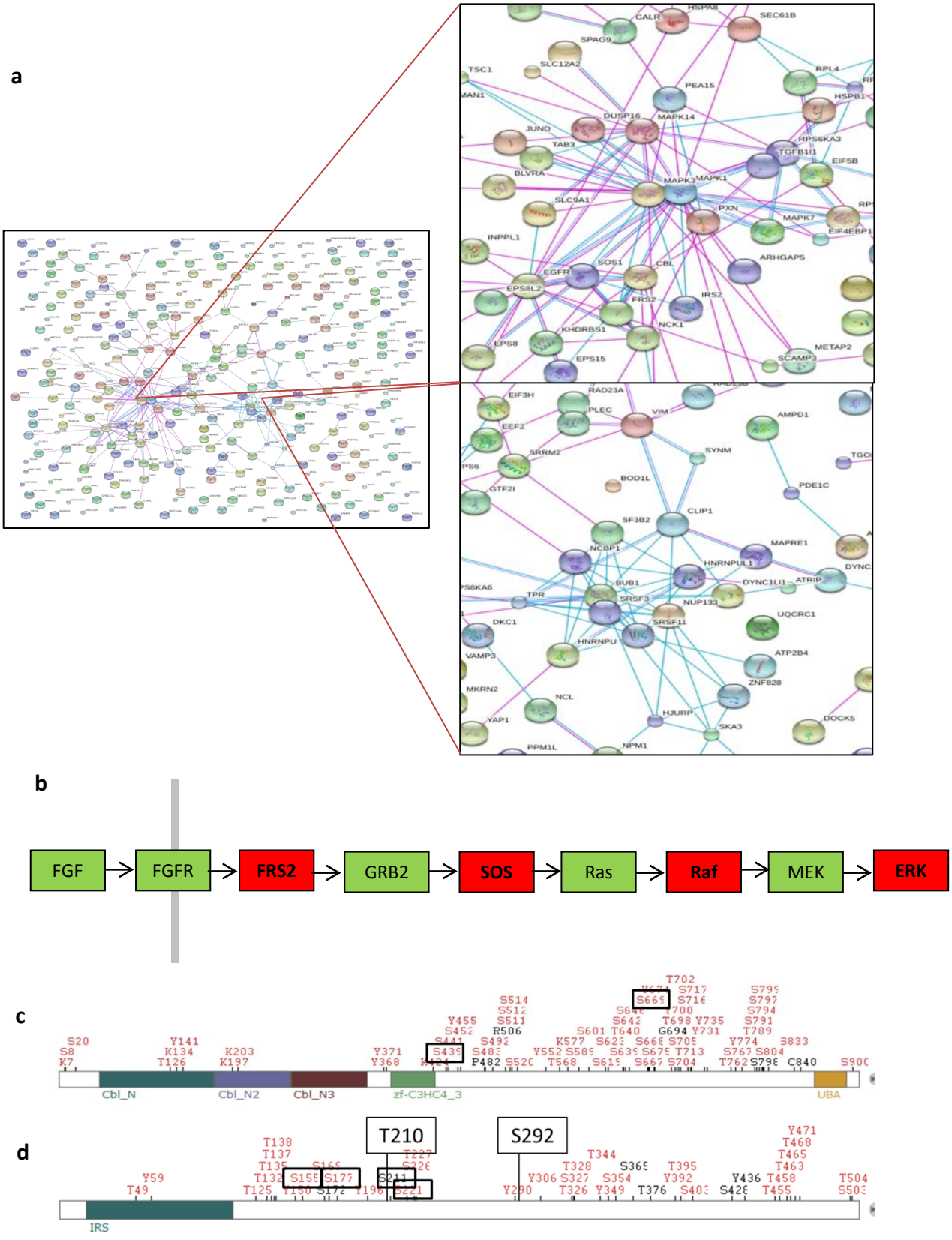

Figure 9 – Analysis of Significantly Lower Phospho-proteins

A – STRING analysis of protein interactions based on high throughput experiments and database evidence. B – FGF induced MAPK pathway. Proteins coloured red had significantly lowered phosphorylation after SU5402 treatment compared to cells without. C - E3 ubiquitin-protein ligase CBL with phosphosites identified as being significantly reduced with application of inhibitors marked in a black box. D - FRS2 (Fibroblast growth factor receptor substrate 2) with phosphosites identified as being significantly reduced with application of inhibitors marked in a black box. Novel phosphosites T210 and S292 also labelled.

To show the in depth individual analysis that can be achieved with the data set two proteins found to be decreased with both inhibitors were chosen to be looked into. The E3 ubiquitin ligase CBL was found at lower phosphorylated levels with both the FGFR and Src inhibitor. The MS data produced found with statistical confidence that one CBL peptide from SU5402 treated cells was phosphorylated at S669 whilst the other peptides found from both showed equal peptide confidence of phosphorylation at S667, S668 or S669 (Figure 9c). All these phosphosites had been found before by proteomic mass spectrometry, with S669 being the most common (phosphosite.org).

FRS2 the direct substrate of FGFR was also found to be significantly lower with both. The peptide found lower with SU5402 was phosphorylated at S221 while the peptide found lower with Dasatinib was phosphorylated at S155 showing that the inhibitors had differing effects on FRS2 (Figure 9d). Two novel phosphorylation sites were found on T210 and S292 but on peptides not found to be changed by treatment with the inhibitors.

ID	Gene Name	Molecular Function	Cellular Component
MAP1B	MAP1 light chain LC1	Structural constituent of cytoskeleton Microtubule binding	Microtubule
DST	Dystonin	Structural constituent of cytoskeleton Calcium ion binding Actin binding	Actin cytoskeleton
MAP2	Microtubule-associated protein 2	Structural constituent of cytoskeleton Microtubule binding	Microtubule
MYO1C	Unconventional myosin-Ic	Motor activity Structural constituent of cytoskeleton Protein binding Enzyme regulator activity	Actin cytoskeleton Cell junction
MAP4	Microtubule-associated protein 4	Structural constituent of cytoskeleton Microtubule binding	Microtubule
MAPK3	MAP kinase-activated protein kinase 3	Protein kinase activity Structural constituent of cytoskeleton Microtubule binding	Microtubule
EHBP1L1	EH domain-binding protein 1-like protein 1	Structural constituent of cytoskeleton Calcium ion binding Actin binding	Actin cytoskeleton
EHBP1	EH domain-binding protein 1	Structural constituent of cytoskeleton Calcium ion binding Actin binding	Actin cytoskeleton
TENS1	Tensin-1	Phosphoprotein phosphatase activity Structural constituent of cytoskeleton Actin binding	Actin cytoskeleton
KRT18	Keratin, type I cytoskeletal 18	Structural constituent of cytoskeleton	Intermediate filament cytoskeleton
CFL1	Cofilin-1	Structural constituent of cytoskeleton Actin binding	Actin cytoskeleton
CFL2	Cofilin-2	Structural constituent of cytoskeleton Actin binding	Actin cytoskeleton
NS1BP IVNS1ABP	Influenza virus NS1A-binding protein	Serine-type peptidase activity Structural constituent of cytoskeleton Transcription factor activity Actin binding Transcription factor activity	Actin cytoskeleton
PXN	Paxillin	Structural constituent of cytoskeleton	Actin cytoskeleton

Table 1 – PANTHER Analysis
Results from PANTHER analysis of proteins significantly reduced in phosphorylation with addition of Dasatinib. Just over 10% were associated with the cytoskeleton.

Titration of PD173074 and Saracatinib

In order to find suitable concentrations of other inhibitors of FGFR and Src that could be used in similar SILAC investigations, titration experiments were performed. The titration required a series of increasing concentrations of the drugs combined with western blots to identify at what point inhibition occurred and how effective it was. This was done using the FGFR inhibitor PD173074 (Mohammadi et al., 1998) and the Src inhibitor Saracatinib (Hennequin et al., 2006). Cells from each amplified FGFR breast cancer cell line were plated into nine separate wells, the first receiving no inhibition or stimulation and the second receiving stimulation by FGF1 and heparin but no inhibition. The remaining seven wells received increasing amounts of the inhibitors before addition of FGF1 and heparin. In the PD173074 titration the concentrations ranged from 50nM to 10μM. As is seen in Figure 10 there is significant inhibition of FGFR at 50nM in all cell lines compared with cells just receiving FGF1 stimulation. Compared with pFGFR with no FGF stimulation, addition of PD173074 significantly reduced activation in SUM52PE and MFM223 at 50nM but not as greatly in CAL120. Both p-ERK and p-AKT were also decreased with addition of the inhibitor while p-Src levels stayed fairly constant.

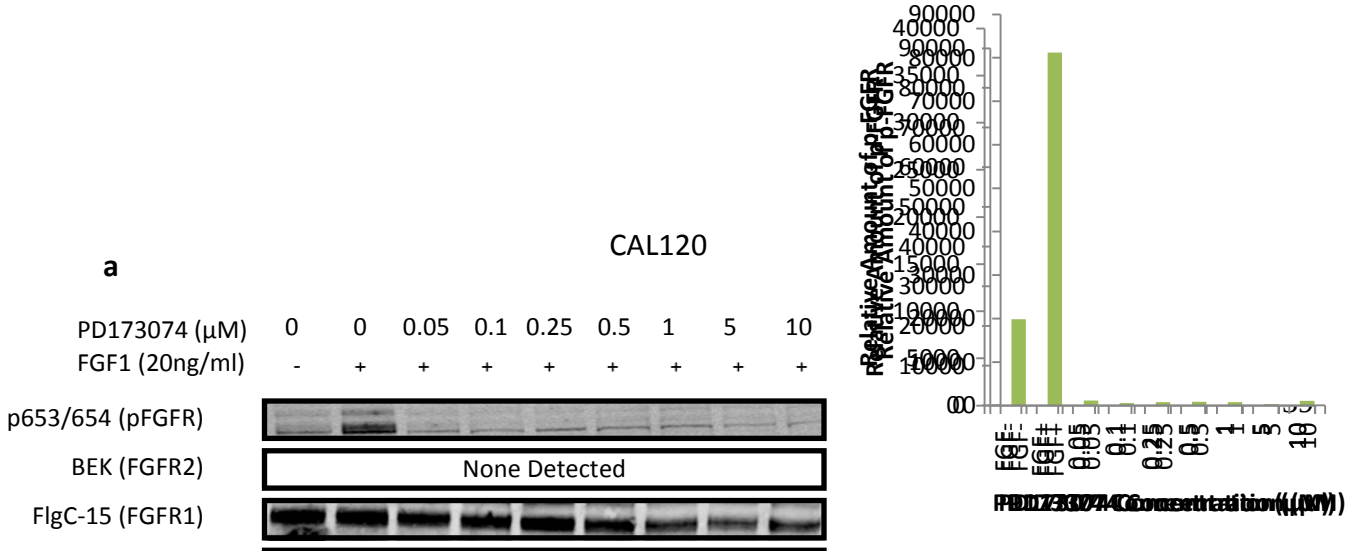

The Saracatinib titration involved a range of 10nM to 10μM and produced clear inhibition of Src at the lowest concentration used (Figure 11). Phosphorylated Src at the Y416 site was decreased to almost half the amount with addition of 10nM of Saracatinib in CAL120 and SUM52PE. Further increases in concentration showed variation with a general decrease only maintained after 1μM. There was no indication of inhibition of pFGFR, pERK or pAKT at any concentration.

In CAL120s levels of FGFR2 detectable with the Bek primary antibody were too low to visualise. P-AKT levels were also very low in CAL120s as well as p-Src levels in MFM223s. Titrations using MCF7 cells were completed but contamination of the samples meant results could not be drawn from the western blots produced.

All quantification was performed using the ImageJ gel analysis method which detects the intensity of the band, taking the area under the curve as a measure of the relative amount of the protein.

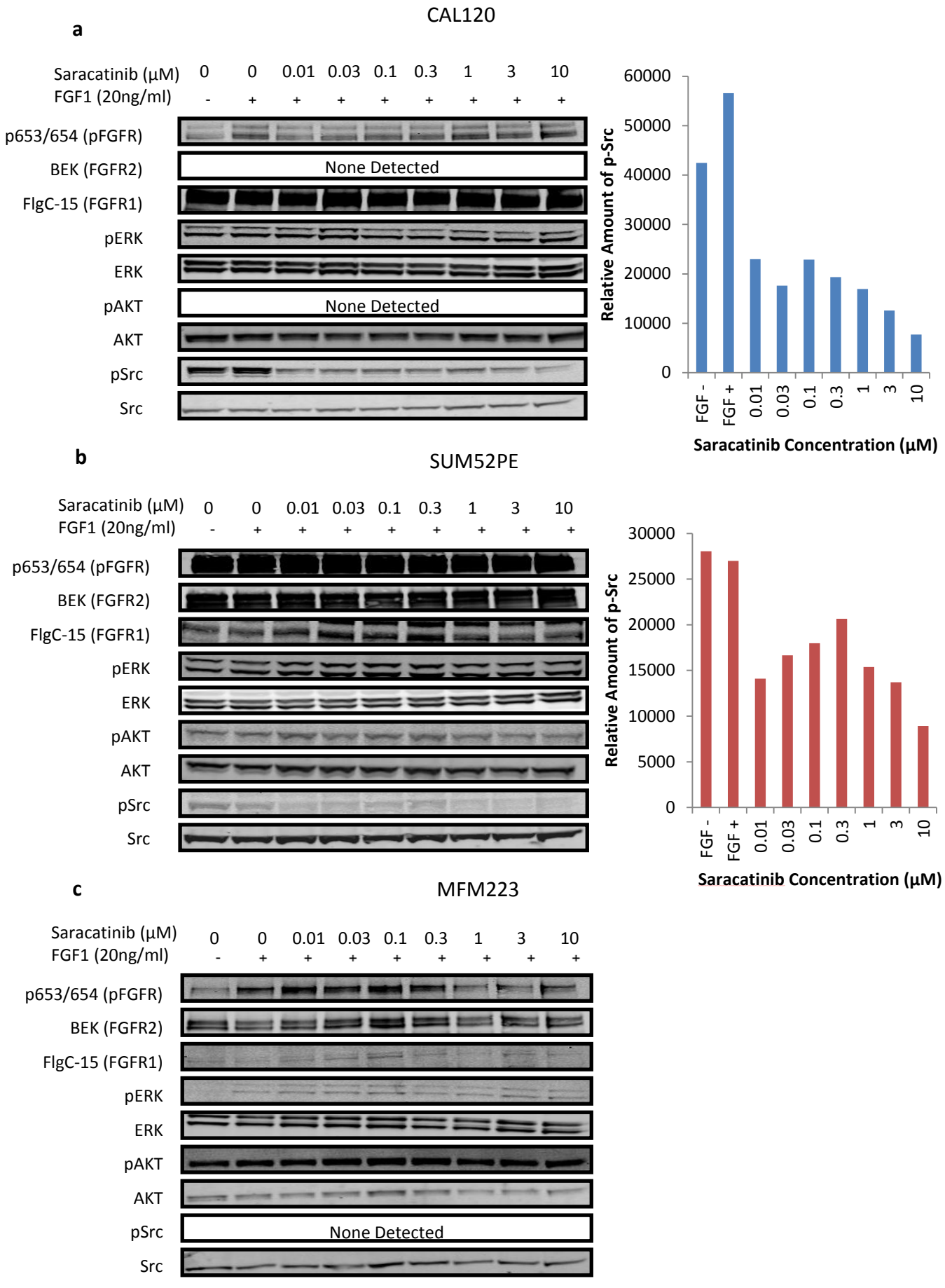

Figure 11 – Saracatinib Titrations

Western blots of total and phosphorylated FGFR, ERK, AKT and Src following inhibition of Src with Saracatinib. Titration ranged from 10nM to 10µM. A – CAL120. B – SUM52PE. C – MFM223. (n=1 for each cell line).

Discussion

A SILAC experiment using FGFR and Src inhibitors on CAL120 breast cancer cells was performed following validation of the function and effectiveness of the drugs via western blotting. Testing of separate FGFR and Src signalling inhibitors was also achieved as well as method development of the phosphoenrichment stage of the SILAC experiment.

SU5402 and Dasatinib Effects on Phosphorylation

SU5402 decreased phosphorylated FGFR at the 653/654 residue in all three cell lines, as well as p-ERK, at a 20μM concentration. Dasatinib had an inhibitory effect on Src at 20nM although this was not accurately quantifiable.

The results showed that SU5402 is an effective inhibitor of FGFR and the decrease in p-ERK indicated that it results in a downstream decrease of the MAPK signalling pathway. No effect on Src was seen with SU5402 addition showing that Src can be activated in other ways than solely by FRS2. This proved that 20μM SU5402 was an ideal concentration for use in the SILAC experiment. The Dasatinib result showed that at the 20nM concentration it is able to reduce phosphorylated Src. However we could not quantify the level of inhibition effectively making it difficult to know if it would be ideal for a SILAC investigation. Due to the low amounts of p-Src in the cell initially requiring high loading and the poor specificity of the antibody the western blots produced were of low quality. To improve this an alternative antibody identifying a different phosphorylated residue on p-Src could be used on a larger scale SDS-PAGE gel.

Phosphoenrichment Method Development

We showed that the 5% ammonium hydroxide/ 5% pyrollidine elution method is more effective in removing phosphopeptides from the Phos-TiO_2 Spin Tips than the 1.75% ammonium hydroxide method . It results in the collection of a larger amount and more diverse selection of phosphopeptides making further analysis of whole cell components more complete. The higher concentration of ammonium hydroxide and addition of pyrollidine produces a more basic environment in the spin tip releasing the more strongly bound phosphopeptides. The greater recovery of some of the known peptides may be due to the phosphorylation occurring on different residues which confers a stronger or weaker ability to bind to the titanium dioxide. To test this the same experiment could be run again but the sample analysed by tandem MS to collect more in depth data on the phosphorylation sites of the peptides.

CAL120 SILAC

Around 10% of phosphopeptides identified were significantly changed with addition of either inhibitor which related to several hundred proteins being present in differing amounts. SU5402 addition lead to the decrease in phosphorylation of several proteins involved in the MAPK signalling pathway as well as RNA processing and transport indicating changes in protein synthesis. Dasatinib addition lead to the decrease in phosphorylation of several proteins assassinated with the cytoskeleton. More in depth analysis was initiated on individual proteins discovered.

More proteins were affected by the SU5402 application than by dasatinib which is representative of the larger network that FGFR signalling has an influence over in comparison to Src. Dasatinib addition resulted in more proteins becoming significantly higher in amount detected compared with SU5402 addition. This may be due to the role Src

plays as a regulator of phosphorylation on certain proteins, with loss of Src resulting in a larger number of phosphorylated proteins than FGFR inhibition.

Phosphorylation of proteins along the MAPK pathway was significantly diminished in CAL120 cells with addition of SU5402 indicating it was strongly affected by the FGFR inhibition. The same statistically significant phosphorylation decrease was not seen in proteins from the other pathways downstream of FGFR suggesting that they were still able to signal at a reasonable level. However with this method of protein detection proteins with a low abundance in the cell initially, which are then further decreased can be difficult to discover. For instance p-Src was not found in the MS runs but the western blots show that it is present in the cells.

The dasatinib effect on cytoskeletal associated proteins may be due to the role Src plays in FGFR signalling. Correct actin cytoskeleton assembly is required for Src/RhoB transport of intracellular FGFR to the membrane (Sandilands et al. 2007). This therefore suggests that loss of phophorylated Src affects cytoskeleton components which it is normally involved in regulating for this role.

Individual analysis found that CBL and FRS2 were decreased in both instances of inhibitor application. CBL can recognize phosphorylated tyrosines on active receptor tyrosine kinases as well as proteins with a Src homology region 2 and 3 (SH2 and SH3) such as Src itself (Thien and Langdon, 2001). Negative regulation of the tyrosine kinase occurs as CBL contains a RING finger domain which recruits ubiquitination enzymes to label the tyrosine kinase for internalisation and degradation. Therefore it is clear to see how the inhibition of

FGFR and Src as well as other tyrosine kinases affected by the drugs could cause a lack of targets for CBL and therefore a decrease in its use and need for phosphorylation.

FRS2 phosphorylation decrease due to SU5402 can easily be explained. Inhibition of FGFR means that the internal tyrosine kinase domains are not phosphorylated and therefore cannot subsequently phosphorylate FRS2 (Eswarakumar et al. 2005). However the reduction caused by Src inhibition is less obvious especially as a decrease in active receptor levels were not seen in the initial western blots or detected in the SILAC experiment. It is suggested that as active Src is normally involved in transport of FGFR to the membrane (Sandilands et al. 2007) its loss would result in active receptor being stranded intracellularly. This would mean the levels of active receptor remained the same but that FRS2 was unable to bind to the receptor in the same way and become phosphorylated at the S155 site. However this loss of FRS2 did not seem to cause disruption of the MAPK or PI3K-AKT pathways it is associated with initiating (Turner and Grose, 2010) This may be due to the S155 phosphorylation site not being required for that role or because Src activation is also involved in ERK signal attenuation (Li et al. 2004) and so without Src, ERK signalling remains. Performing the experiment again but allowing a longer time to elapse following FGF stimulation may show ERK levels dropping and indicate that the second explanation is correct but the lack of other proteins involved in the MAPK or PI3K-AKT pathway, being significantly lower in the SILAC data set, suggests not.

Titration of PD173074 and Saracatinib

The titration experiments using PD173074 and Saracatinib found that at 50nM PD173074 significantly reduced phosphorylated FGFR at a specific site and that Saracatinib did the same at 10nM with p-Src.

The decreased p-ERk and p-AKT levels in the PD173074 titration also indicated reduced MAPK and PI3K-AKT signalling, presumably as a consequence of a decrease in FGFR signalling. The greater effect of the drug on SUM52PE and MFM223 is likely due to the higher ligand independent FGFR activation occurring in the FGFR2 amplified cell lines. A 50nM concentration would be ideal for use in a SILAC experiment to ensure inhibition, however another titration at lower concentrations would be interesting as the reported IC_{50} of PD173074 for FGFR1 is 21.5nM (Mohammadi et al., 1998) suggesting that there may be a more efficient concentration between the two.

The results of the Saracatinib titration show that MAPK and PI3K-AKT signalling was not reduced. Inhibition in CAL120s was around 50% at 10nM and although it seemed similar in the SUM52PEs the levels of p-Src were very low making quantification unreliable which may explain the variation seen. The reported IC_{50} of Saracatinib for Src is 2.7nM (Hennequin et al., 2006) however our data suggests that this may not be the case in these cell lines. Repetition with an alternative p-Src antibody as well as a wider titration range would help to find an ideal concentration for further work with Saracatinib.

Future work

In order to progress this work performing the same SILAC experiment again with CAL120s and comparing the results would provide a much clearer picture of the changes occurring.

Cunningham et al. (2010) reported finding only a 50% overlap between SILAC experiments so a repeat would be essential to take the data further and gain a more reliable picture of the proteomics affected. Switching which inhibitors are added to which labelled cells and comparing the results would also point out if the labelling had any effects on the biological processes.

The data collected by this investigation was too vast to undergo a full analysis of the possible connections. The proteins showing no obvious direct interactions or functional groupings require individual in depth analysis to provide a much more detailed map of the phosphorylation events downstream of FGFR and Src. Results found in the SILAC experiments can be validated by straight western blots if antibodies for the specific phosphosites exist. If not anti-phospho immunoprecipitation (IP) experiments can be performed to validate. Building up the data found with data collected from other SILAC experiments on similar cell lines and with different inhibitors will allow a molecular map of the individual breast cancer cell lines to be created. This will result in a more detailed breast cancer diagnosis and allow for treatment to be specialised to a patient.

References:

1. Brooks AN, Kilgour E, Smith PD. (2012) Molecular pathways: fibroblast growth factor signaling: a new therapeutic opportunity in cancer. Clin Cancer Res. 18(7): 1855-1862.
2. Cox J–and Mann M. (2008) MaxQuant enables high peptide identification rates, individualized p.p.b.-range mass accuracies and proteome-wide protein quantification. Nature Biotechnology. 26: 1367-1372
3. Cox J, Neuhauser N, Michalski A, Scheltema RA, Olsen JV and Mann M. (2011) Andromeda: A Peptide Search Engine Integrated into the MaxQuant Environment. J. Proteome Res. 10(4): 1794–1805
4. Cunningham DL, Sweet SM, Cooper HJ, and Heath JK. (2010) Differential Phosphoproteomics of Fibroblast Growth Factor Signaling: Identification of Src Family Kinase-Mediated Phosphorylation Events. J Proteome Res. 9(5): 2317–2328.
5. Eswarakumar VP, Lax I, Schlessinger J. (2005) Cellular signaling by fibroblast growth factor receptors. Cytokine Growth Factor Rev. 16(2): 139-149.
6. Ethier SP, Kokeny KE, Ridings JW, Dilts CA. (1996) erbB family receptor expression and growth regulation in a newly isolated human breast cancer cell line. Cancer Res. 56(4): 899-907.
7. Gelsi-Boyer V, Orsetti B, Cervera N, Finetti P, Sircoulomb F, Rougé C, Lasorsa L, Letessier A, Ginestier C, Monville F, Esteyriès S, Adélaïde J, Esterni B, Henry C, Ethier SP, Bibeau F, Mozziconacci MJ, Charafe-Jauffret E, Jacquemier J, Bertucci F, Birnbaum D, Theillet C, Chaffanet M. (2005) Comprehensive profiling of 8p11-12 amplification in breast cancer. Mol Cancer Res. 3(12): 655-667.
8. Hackenberg R, Lüttchens S, Hofmann J, Kunzmann R, Hölzel F, Schulz KD. (1991) Androgen sensitivity of the new human breast cancer cell line MFM-223. Cancer Res. 51(20): 5722-5727.
9. Hart KC, Robertson SC, Kanemitsu MY, Meyer AN, Tynan JA, Donoghue DJ. (2000) Transformation and Stat activation by derivatives of FGFR1, FGFR3, and FGFR4. Oncogene. 19(29): 3309-3320.
10. Hennequin LF, Allen J, Breed J, Curwen J, Fennell M, Green TP, Lambert-van der Brempt C, Morgentin R, Norman RA, Olivier A, Otterbein L, Plé PA, Warin N, Costello G. (2006) N-(5-chloro-1,3-benzodioxol-4-yl)-7-[2-(4-methylpiperazin-1-yl)ethoxy]-5- (tetrahydro-2H-pyran-4-yloxy)quinazolin-4-amine, a novel, highly selective, orally available, dual-specific c-Src/Abl kinase inhibitor. J Med Chem. 49(22): 6465-6488.
11. Jackson CC, Medeiros LJ, Miranda RN. (2009) 8p11 myeloproliferative syndrome: a review. Hum Pathol. 41(4): 461-476.
12. Kovalenko D, Yang X, Nadeau RJ, Harkins LK, Friesel R. (2003) Sef inhibits fibroblast growth factor signaling by inhibiting FGFR1 tyrosine phosphorylation and subsequent ERK activation. J Biol Chem. 278(16): 14087-14091.
13. Li C, Scott DA, Hatch E, Tian X, Mansour SL. (2007) Dusp6 (Mkp3) is a negative feedback regulator of FGF-stimulated ERK signaling during mouse development. Development. 134(1): 167-176.
14. Li X, Brunton VG, Burgar HR, Wheldon LM, Heath JK. (2004) FRS2-dependent SRC activation is required for fibroblast growth factor receptor-induced phosphorylation of Sprouty and suppression of ERK activity. J Cell Sci. 117(25): 6007-6017.
15. Lombardo LJ, Lee FY, Chen P, Norris D, Barrish JC, Behnia K, Castaneda S, Cornelius LA, Das J, Doweyko AM, et al. (2004) Discovery of N-(2-chloro-6-methyl-phenyl)-2-(6-(4-(2-hydroxyethyl)-piperazin-1-yl)-2-methylpyrimidin-4-

ylamino)thiazole-5-carboxamide (BMS-354825), a dual Src/Abl kinase inhibitor with potent antitumor activity in preclinical assays. J Med Chem. 47: 6658–6661.
16. Mann M, Ong SE, Grønborg M, Steen H, Jensen ON, Pandey A. (2002) Analysis of protein phosphorylation using mass spectrometry: deciphering the phosphoproteome. Trends Biotechnol. 20(6): 261-268.
17. Mann M. (2006) Functional and quantitative proteomics using SILAC. Nat Rev Mol Cell Biol. 7(12): 952-958.
18. Martínez N, García-Domínguez CA, Domingo B, Oliva JL, Zarich N, Sánchez A, Gutiérrez-Eisman S, Llopis J, Rojas JM. (2007) Sprouty2 binds Grb2 at two different proline-rich regions, and the mechanism of ERK inhibition is independent of this interaction. Cellular Signalling. 19(11): 2277–2285.
19. Mohammadi M, Froum S, Hamby JM, Schroeder MC, Panek RL, Lu GH, Eliseenkova AV, Green D, Schlessinger J, Hubbard SR. (1998) Crystal structure of an angiogenesis inhibitor bound to the FGF receptor tyrosine kinase domain. EMBO J. 17(20): 5896-5904.
20. Mohammadi M, McMahon G, Sun L, Tang C, Hirth P, Yeh BK, Hubbard SR, Schlessinger J. (1997) Structures of the tyrosine kinase domain of fibroblast growth factor receptor in complex with inhibitors. Science. 276(5314): 955-960.
21. Mohammadi M, Olsen SK, Ibrahimi OA. (2005) Structural basis for fibroblast growth factor receptor activation. Cytokine Growth Factor Rev. 16(2): 107-137.
22. Olsen JV, Ong SE, Mann M. (2004) Trypsin cleaves exclusively C-terminal to arginine and lysine residues. Mol Cell Proteomic. 3(6): 608-614.
23. Powers CJ, McLeskey SW, Wellstein A. (2000) Fibroblast growth factors, their receptors and signaling. Endocr Relat Cancer. 7(3): 165-197.
24. Sandilands E, Akbarzadeh S, Vecchione A, McEwan DG, Frame MC, Heath JK. (2007) Src kinase modulates the activation, transport and signalling dynamics of fibroblast growth factor receptors. EMBO Rep. 8(12): 1162-1169.
25. Schlessinger J, Plotnikov AN, Ibrahimi OA, Eliseenkova AV, Yeh BK, Yayon A, Linhardt RJ, Mohammadi M. (2000) Crystal structure of a ternary FGF-FGFR-heparin complex reveals a dual role for heparin in FGFR binding and dimerization. Mol Cell. 6(3): 743-750.
26. Soule HD, Vazquez J, Long A, Albert S, and Brennan M. (1973) A Human Cell Line From a Pleural Effusion Derived From a Breast Carcinoma. J Natl Cancer Inst. 51(5): 1409-1416.
27. Steen H, Mann M. (2004) The ABC's (and XYZ's) of peptide sequencing. Nat Rev Mol Cell Biol. 5(9): 699-711.
28. Taylor JG, Cheuk AT, Tsang PS, Chung JY, Song YK, Desai K, Yu Y, Chen QR, Shah K, Youngblood V, Fang J, Kim SY, Yeung C, Helman LJ, Mendoza A, Ngo V, Staudt LM, Wei JS, Khanna C, Catchpoole D, Qualman SJ, Hewitt SM, Merlino G, Chanock SJ, and Khan J. (2009) Identification of FGFR4-activating mutations in human rhabdomyosarcomas that promote metastasis in xenotransplanted models. J Clin Invest. 119(11): 3395–3407.
29. Thien CB, Langdon WY. (2001) Cbl: many adaptations to regulate protein tyrosine kinases. Nat Rev Mol Cell Biol.2(4): 294-307.
30. Turner N, Grose R. (2010) Fibroblast growth factor signalling: from development to cancer. Nat Rev Cancer. 10(2):116-129.
31. Turner N, Lambros MB, Horlings HM, Pearson A, Sharpe R, Natrajan R, Geyer FC, van Kouwenhove M, Kreike B, Mackay A, Ashworth A, van de Vijver MJ, Reis-Filho. (2010) Integrative molecular profiling of triple negative breast cancers

identifies amplicon drivers and potential therapeutic targets. Oncogene. 29(14): 2013-2023.
32. Turner N, Pearson A, Sharpe R, Lambros M, Geyer F, Lopez-Garcia MA, Natrajan R, Marchio C, Iorns E, Mackay A, Gillett C, Grigoriadis A, Tutt A, Reis-Filho JS, Ashworth A. (2010) FGFR1 amplification drives endocrine therapy resistance and is a therapeutic target in breast cancer. Cancer Res. 70(5): 2085-2094
33. Webster MK, Donoghue DJ. (1997) FGFR activation in skeletal disorders: too much of a good thing. Trends Genet. 13(5): 178-182.
34. Wesche J, Haglund K, Haugsten EM. (2011) Fibroblast growth factors and their receptors in cancer. Biochem J. 437(2): 199-213.
35. Wong A, Lamothe B, Lee A, Schlessinger J, Lax I. (2002) FRS2 alpha attenuates FGF receptor signaling by Grb2-mediated recruitment of the ubiquitin ligase Cbl. Proc Natl Acad Sci U S A. 99(10): 6684-6689.

Analysing lymphocyte populations and CD52 intensity of stem cell transplant bags and during early immune reconstitution following allogeneic stem cell transplantation.

Luke Maggs
MRes Molecular and Cellular Biology

Abstract

Haematopoietic stem cell transplantation is a last resort treatment to cure many haematological malignancies. Stem cells collected from a donor are infused into the patient following chemo/radiotherapy treatment. The graft verses leukaemia response is essential for remission to occur but is likely to result in a graft versus host disease (GvHD) side effect. Campath, a CD52 specific monoclonal antibody, is used as a GvHD preventative measure as it reduces the T lymphocytes responsible for the effect. Comparison of the immune system cell populations present in the transplanted cells have not been tested to see if they are the same as a healthy donor, or how they change during the first two weeks post-transplantation. Our findings indicate that the ratios of T, B and NK lymphocytes are different in the transplanted cells compared to healthy blood and that CD8 and CD4 T cells reach a roughly 1:1 ratio. CD52 intensity was also dimmed in all cell types before transplantation, although campath was still able to reduce cell numbers, affecting T and B lymphocytes with higher CD52 densities than NK cells. Post-transplantation NK cells become the dominant lymphocyte cell population conferring a GvL response and restricting GvHD.

Contents

Introduction

The Immune system

The body's immune system defends against infection and disease by identifying foreign molecules and attempting to eliminate them, as well as providing a memory of past diseases in order to act more swiftly against re-infection. Upon infection the innate immune response, an evolutionarily conserved mechanism, acts in a generalised manner to destroy foreign bodies whilst the adaptive immune response, which is only found in higher vertebrates, acts with a much more specialised approach.

The innate system comprises of macrophages, granulocytes, mast cells and dendritic cells. Macropahges, granulocytes and dendritic cells are all phagocytes, but with varying functions. Macrophages engulf and destroy invading microorganisms as well as clearing up dead material found in tissues. They are also used to trigger the inflammatory response and signal for other immune system cells to accumulate at the site of infection (Martinez et al., 2008). Granulocyes are relatively short lived and contain cytoplasmic granules of digestive enzymes and substances used to destroy the cells they engulf. Dendritic cells are also known as antigen presenting cells (APCs) due to their ability to engulf a foreign body, break it down into peptides and present the peptides on their surface. Natural killer (NK) cells (discussed in more detail later) are also part of innate immunity despite being derived from the same lymphoid progenitor as the adaptive immune system T and B cells. NK cells act in a non-specific manner against abnormal cells and as their name suggests destroys them. The innate response is important to combat infection initially and give the body time to develop an adaptive immune response in order to eliminate the infection entirely.

The adaptive immune system provides a far more specialised response against invading foreign material and can produce a long lasting defence against that specific pathogen. It is stimulated by the pathogens and the innate immune response produced, which causes release

of cytokines to activate adaptive immune system cells and to present them with foreign antigens. (Figure 1). The adaptive immune system antibody response is mediated by B cells which detect foreign antigens and produce specific immunoglobulins against them. These immunoglobulins bind to the antigen and block the pathogen from functioning as well as targeting the cell for destruction by cells of the innate system (Alberts et al., 2008). T cells provide the other side of the adaptive immune response as they recognise cells presenting foreign antigens on their surface and can destroy them (Alberts et al., 2008)). T and B cells (discussed in more detail later) are lymphocytes which circulate the body via the blood and lymph systems and accumulate at lymphoid tissues in a naive form until they encounter their specific antigen and become activated. B lymphocytes are formed in the bone marrow and upon activation produce antibodies specific to the activating antigen (Blom and Spits, 2006). Precursor T lymphocytes are also produced in the bone marrow but migrate to the thymus where they mature (Blom and Spits, 2006).

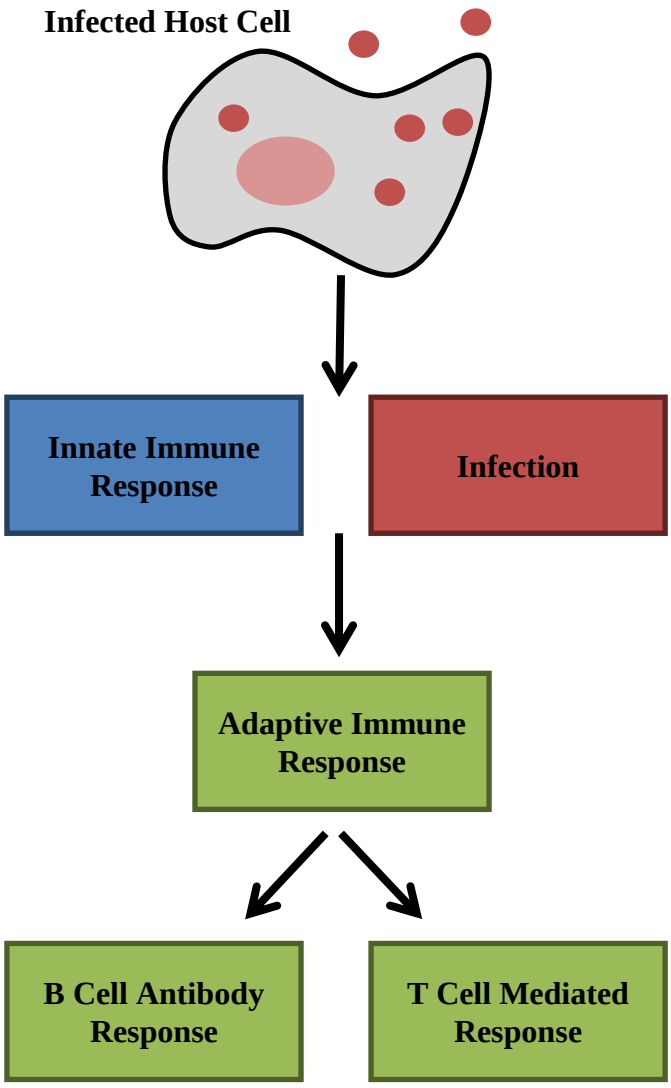

Figure 1 – Immune Response (Adapted from Alberts et al., 2008)
Infection triggers the innate immune response which together with antigens on the pathogens triggers the adaptive immune response. The two main arms of the adaptive immune response are the production of antigen specific antibodies by B cells and pathogen targeted killing by T cells.

Generation of an adaptive immune response

Dendritic cells provide a connection between the innate and adaptive immune systems as immature cells can take up a foreign body and present peptides from it on its surface using major histocompatibility complex (MHC) class II molecules. This mature dendritic cell migrates to lymphoid tissues where it expresses high levels of co stimulatory molecules CD80 and CD86 and presents the peptides to T cells of the adaptive immune system (Lim et al., 2012). If any of the peptides presented provide an antigen for the lymphocytes to detect, then with the help of the co stimulatory molecules it can cause T cell activation. Upon

activation by dendritic cells they proliferate and differentiate into either cytotoxic T lymphocytes (CTL) which can kill cells, helper T cells (Th), which signal to other cells, or regulatory T cells (Treg), which can control immune responses (Murphy et al., 2012).

The production of Th cells assists B cells to produce an effective antibody response (Ma et al., 2012). The activated effector T and B lymphocytes undergo clonal expansion creating a huge increase of cells. Most of these then exit the lymphoid tissue via the bloodstream and travel to the site of infection where they will act in the case of T cells, or migrate to the bone marrow and secrete antibodies from there into the blood stream, in the case of B cells (Shulman et al., 2011; Murphy, 2012). The antibodies will bind to the antigens and mark the presence of the foreign bodies indicating the need for them to be destroyed. Eventually most of these cells will die, however a few memory cells will remain in order to provide a more rapid response to that antigen should it be encountered again (Gray, 2002).

Each lymphocyte produced differs in its antigen receptor to others via a process of gene segment rearrangement (Jaeger et al., 2013). This allows the immune system to detect any possible antigen which could present itself. When a lymphocyte is activated it proliferates in a clonal manner, creating more cells with the same antigen receptor so the antigen can be detected/eliminated throughout the body quicker. This clonal expansion takes time though which is why the innate immune response is so important.

The immune system cell types are interlinked, and so detecting the levels of each of them and their subgroups under differing circumstances will provide an interesting account of the immune system response to those conditions.

T cells

T cells represent the majority (70-75%) of peripheral blood lymphocytes. There are two main classes of T lymphocytes, those which express CD8 and those which express CD4. Both

recognise antigens on cells but act in differing ways upon recognition. CD8 cells are broadly classed as cytotoxic T lymphocytes and can kill infected cells. CD4 cells are T helper cells which can activate cells such as B cells to produce antibodies more effectively (Murphy et al., 2012).

Major histocompatibility complex (MHC) molecules are proteins which during their synthesis incorporate a peptide into their structure and then present the peptide on the surface of the cell as an antigen for detection. MHC class I molecules are found on most cell types and collect peptides from proteins made in the cytosol. They are recognised by CD8 T cells (Viret and Janeway, 1999). MHC class II molecules are more specific and are only found on some cells of the immune system, in particular APCs. They collect peptides from proteins in intracellular vesicles (e.g. proteins engulfed by APCs) and are recognised by CD4 T cells (Holling et al.,2004).

The T cell receptor which consists of an a/b TCR heterodimer and three CD3 chains is present on all T cells. It is able to recognise a peptide presented by a MHC molecule but requires CD4 or CD8 if the MHC is class II or class I respectively in order to produce intracellular signalling and therefore a response. Binding of CD4/CD8 to the MHC can activate the src family kinase Lck associated with the intracellular CD4/CD8 domain. Lck is able to cause tyrosine phosphorylation of the cytoplasmic regions of the CD3 chains (ITAMs – immunoreceptor tyrosine based activation motifs) which provides sites for SH2 domains of downstream signalling proteins to bind. CD4/CD8 are also thought to stabilise the peptide:MHC complex interaction and allow more time for signalling to occur (Smith-Garvin et al., 2009).

T and B cells enter lymph or infected tissue via the blood. The capillaries or equivalent in lymph nodes secrete molecules, which T and B cells have receptors for so they adhere and move into the tissue. For example the chemokine CCL21 is released which is recognised by

the chemokine receptor CCR7 found on naive T cells allowing them entry into the lymph nodes. CCR7 is also characteristic of central memory T cells (Sallusto et al., 2004). CD45RA is another marker of naive T cells as upon activation it is replaced by the CD45RO isoform (Akbar et al., 1988). CD45RA however is also a marker of a subset of effector memory T cells.

B Cells

The B cells require CD19, a B cell specific co receptor protein which can enhance B cell receptor signalling, for activation (Depoil et al., 2008). Upon activation B cells can differentiate into plasma cells, which produce antibodies, or memory cells of which CD27 is a marker (Agematsu et al., 2000). Initially all naive B cells express IgM and IgD. However upon activation B cells are able to undergo immunoglobulin class switching to another subtype via DNA recombination. Transitional B cells mark the step between immature bone marrow B cells and mature circulating B cells and can be identified by the expression of high levels of CD24 and CD38 (Sims et al., 2005). Finally plasmablasts which are the precursors to plasma cells are identified by high levels of CD27 and CD38 a marker of early B cells (Mei et al., 2007).

Natural Killer Cells

Natural killer cells make up 10-15% of the peripheral blood lymphocytes of healthy donors and can lyse cells by releasing cytotoxic granules. They do not have a varying receptor like T and B cells but are able to recognise infected or transformed cells via changes in MHC molecules (Murphy et al., 2012). NKs are characterised as being CD56 positive (NK marker - isoform of neural cell adhesion molecule (NCAM)) and CD3 negative (T cell marker - associated with T cell receptor). The level of CD56 on the cells can be split into CD56 bright

(~10%) which are considered the cytokine producing cells and are able to influence immune response, and CD56 dim (~90%) which possess the cytotoxic NK function (Vivier et al., 2008). Stimulatory and inhibitory receptors on the surface of NK cells control the activity of the cells by engaging with ligands including MHC class I molecules, MHC class I-like molecules and molecules unrelated to MHC. There are three super families of NK receptors. The killer cell immunoglobulin like receptors (KIRs) are one such family of which the intracellular domains of the receptors confer their inhibitory or activating function. A long cytoplasmic domain indicates an inhibitory, MHC class I recognition, function, or a short domain indicates a stimulatory function (Radaev and Sun, 2003). A balance between the two is required to regulate NK function and all NKs contain at least one inhibitory receptor to ensure tolerance. It is suggested that over time CD56 bright cells develop into CD56 dim cells and that their function changes as they lose their dense CD56 and NKG2A positive phenotype and acquire more KIRs and a NKG2C phenotype, gaining a cytotoxic function (Caligiuri, 2008). Eventually they become memory NK cells and acquire CD27.

Stem Cell Transplant and GvHD

Haematological malignancies are cancers which affect the blood, bone marrow and lymph systems such as leukaemia and lymphomas. The cancerous cells cause uncontrolled growth and therefore a decrease in healthy cell functionality, resulting in reduced effectiveness of the blood and immune systems, which will ultimately lead to death unless intervention is taken. Treatment involves chemotherapy and/or radiotherapy to destroy the cancerous cells, however this is not always effective. For many patients allogeneic haematopoietic stem cell transplantation (HSCT) is the last or only treatment available to cure their disease. A sibling

or matched unrelated donor is required to donate the stem cells due to complications with transplant rejection.

Collection of stem cells from the donor usually involves treating them with a five day course of granulocyte colony-stimulating factor (G-CSF) to induce proliferation of stem cells. These are then collected from the donor's peripheral blood via a process of apheresis which involves removal of blood from the patient into a centrifuge inside which the blood is separated into layers. The leukocyte layer is then taken off while the remaining blood is circulated back into the donor (Reddy et al., 2005). The sample can then be stored for up to a day without greatly affecting cell viability (Sugrue et al., 1998). The recipient begins a course of high dosage chemotherapy and/or radiotherapy a week before the transplantation to destroy cancerous as well as normal bone marrow cells in order to provide room for the graft. The donor stem cells are then transplanted into the patient, via a drip, where they will hopefully stimulate production of new healthy blood cells.

As stated above MHC molecules are required to present antigens on the surface of cells and indicate to T lymphocytes which cells are part of the body and which are not. MHCs in humans are encoded by a selection of genes known as human leukocyte antigens (HLA) which possess a large number of alleles resulting in wide variation throughout the population (Murphy et al., 2012). This is a problem when performing transplants between people as the immune system, specifically the T cells, recognises that the cells are not 'self' and so activates an allo-immune response against them. This was first shown in mice as a skin graft onto a normal mouse was rejected, but a graft onto a nude mice, depleted of T cells, survived, with rejection stimulated again by addition of normal T cells (Kindred, 1974). Therefore matching of the major histocompatibility antigens (HLA-A,-B,-C,-DR,-DP and D-Q) is important in graft survival, however a perfect match between the minor antigens is rarely

possible even between siblings. Improvements in immunosuppressive treatments have helped to solve this problem for most types of transplant, however allogenic stem cell transplantation produces further complications (Murphy et al., 2012).

Despite the attempts to match major antigens there is likely to be differences between the minor antigens present on donor and recipient cells. This has a useful effect as the transplanted donor T cells are able to confer a graft versus leukaemia (GvL) response and destroy residual malignant cells in the patient (Horowitz et al., 1990). This is due to haematopoiesis-restricted minor histocompatibility antigens such as HA-1 on host cells (Marijt et al., 2003). This is an essential process in the curative nature of the HSCT. However a side effect called graft versus host disease (GvHD) is almost certain to occur in some form where in contrast to GVL non haematopoietic cells are targeted. The chemo/radiotherapy treatment the patient receives damages tissues, and the activation of donor T cells due to the minor antigen mismatch, results in secretion of inflammatory cytokines (Figure 2) (Reddy, 2003). This causes the production of chemokines which recruit CXCR3+ transplanted T lymphocytes into patient tissues such as the skin, gut and liver where they begin to attack healthy cells (Piper et al., 2007; Croudace et al., 2012). This occurs in 20-80% of HSCT patients depending on associated risk factors such as the level of mismatch, age, sex and cytomegalovirus infection (Weisdorf et al., 1991). In acute GvHD, which develops within 2-3 weeks post-transplant, symptoms begin as a rash on the hands and feet or face and can develop into gastrointestinal and liver problems. GvHD can be mild or severe and last from weeks, to months, to years and in some cases can be life threatening. However the presence of GvHD indicates the immune system is active and is associated with more effective GvL response. Therefore acquiring a suitable balance between the two or attempting to maintain the GvL whilst reducing the chance of GvHD is an important area of research.

One method of doing this is to apply a conditioning regiment to the patient in the week before they receive their transplant to try and reduce the number of mature T cells which will cause GvHD, after the donor cells are transferred in the graft. Campath-1H (Alemtuzumab) is a humanized CD52 monoclonal antibody which is used for this purpose (Kanda et al., 2011). CD52 is found on T and B lymphocytes, a majority of monocytes, macrophages, NK cells, and a subpopulation of granulocytes, as well as spermatozoa (Domagała and Kurpisz. 2001). However the actual role of CD52 on lymphocytes is as of yet unknown. Campath is able to induce cell mediated lysis of lymphocytes (Hale et al., 1983) and has been shown to provide a reduced GvHD response in patients (Waldmann et al., 1984). It is therefore in use as a GvHD preventative measure in institutions providing HSCT, with a usual dose of 10mg per day for five days prior to transplant.

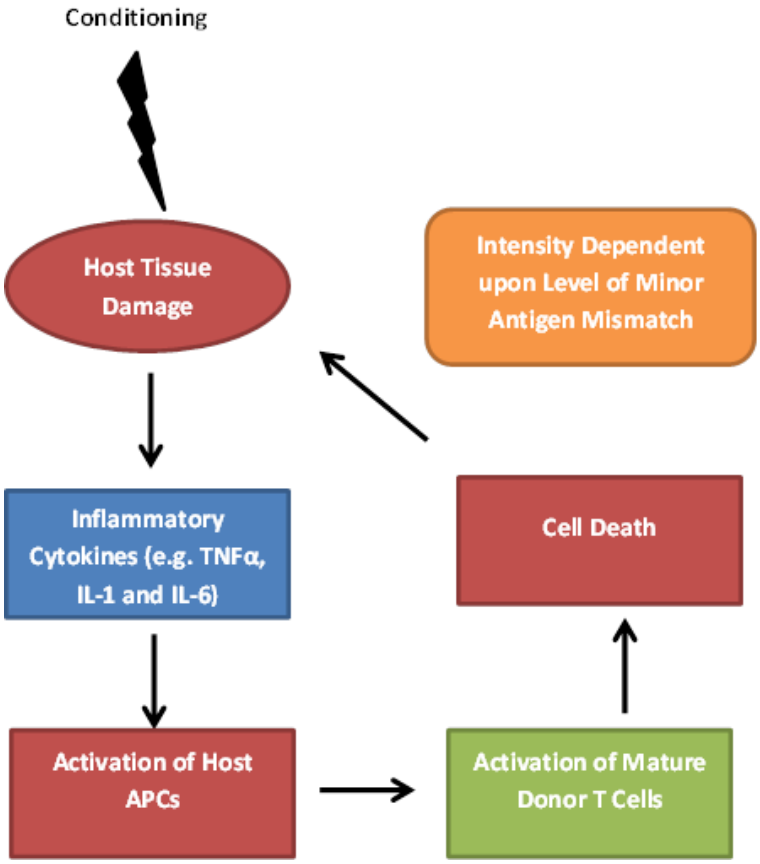

Figure 2 - GVHD Pathophysiology (Adapted from Ferrara et al., 2009)
Chemotherapy and/or radiotherapy treatment damages host tissues resulting in inflammation and the release of inflammatory cytokines. These cytokines increase activation of host APCs which therefore present more

antigens to the mature donor cells. Activated T lymphocytes proliferate and differentiate to produce cytotoxic T cells which cause the GvHD tissue damage. A greater difference in minor antigen matching will produce a larger mature T cell activation population and therefore a greater GvHD response.

Areas of Interest

Current research involves understanding how the patient's immune cell population recovers following HSCT (Torelli et al., 2011) and how Campath can be optimised to prevent GvHD (Kanda et al., 2011). Rao et al., (2012) looked at the cytolytic effect of Campath on specific immune cells with differing CD52 cell surface densities in vitro. They found that in some cells, mainly of the adaptive immune system, that Campath's cytolytic effect was in direct correlation with the CD52 density on the cells, as B and T cells with high CD52 densities were more effectively killed than NK cells which expressed lower CD52 density. They also found that some cells, myeloid dendritic cells and monocytes, were less susceptible to Campath killing despite having high CD52 densities and it was suggested this was down to resistance mediated by high expression levels of complement inhibitory proteins.

We are interested in how this differential expression relates to patients during HSCT and how differences in the impact of Campath upon cell death may influence immune reconstitution following transplantation, in particular during the first two weeks (Very Early Immune Reconstitution - VEIR). How the immune system recovers following HSCT is an important factor in the development of GvHD. Croudace and Inman (2013 - unpublished) have shown correlations between specific T cell subpopulation recovery and GvHD during VEIR. Chan (2013 – unpublished) has also discovered similar correlations in the NK sub populations. It has also been shown that NK cells which usually represent ~10% of lymphocytes in healthy blood become the dominant cell population during VEIR following HSCT, whilst T cell frequencies and numbers remain low. This may be due to the differing effects of Campath on these cell types.

To explore the effects of Campath in HSCT and upon VEIR we firstly examined if the cells entering a patient at day 0 were the same as from a healthy donor. To do this we compared T

and NK cells present in the stem cell collection from the donor with cells from healthy donors. It is considered that the immune system cell populations in the transplant bag are similar to those from the PBMC of a healthy donor, however this has not yet been formally shown. We therefore compared the cellular profiles of the stem cell bags with healthy donors PBMC to see if the same percentages of cells were present and if there were any alterations in the properties of these cells. We then studied how these cellular populations changed over the first two weeks post-transplant. Also as an indication of the cellular susceptibility of lymphocyte populations to Campath, the density of CD52 on the cell surface was also studied. To try and determine how much of an impact Campath produced on changes in cell populations during VEIR, experiments to test its functionality *in vitro* were initiated.

Materials and Methods

Patient Cohort and Sample Collection

Patients undergoing allogeneic stem cell transplant (SCT) for haematological malignancies at the Queen Elizabeth Hospital Birmingham were incorporated onto the study after fully informed written consent was given, prior to receipt of stem cells (ethics code: 051Q7071175). The empty stem cell bags were received at day 0 post SCT and up to 50 ml peripheral blood was taken on days 2, 7 and 14 post SCT. Ten patients were followed during VEIR, with six receiving stem cells from a matched unrelated donor and four from a sibling. All but one received the standard CAMPATH dose of 10mg per day for five days. Patients had varying conditioning regimes dependent on their situation (See Table 1 for full patient details). Healthy donors used as controls were informed of the use of their samples and consented to give up to 30 ml peripheral blood.

PBMC Extraction

Blood was collected in anticoagulant coated vacuum tubes and diluted 1:1 with RPMI media (Sigma). The diluted blood was then layered at a 2:1 ratio of blood to Lymphoprep^{TM} (Stemcell^{TM} Technologies), and centrifuged at 1994rpm for 25 minutes without the use of the brake to produce separation through the density gradient medium. The PBMC layer (containing lymphocytes, monocytes and macrophages) was then extracted using a Pasteur pipette and washed several times with RPMI media or MACS buffer, before staining or addition of freezing media (10% Dimethyl sulfoxide (DMSO) (Sigma) with Foetal Calf Serum (FCS) (BioSera)), and subsequent gradual freezing to -80^{o}C.

Stem Bag Sample Extraction

Empty transplant stem cell bags which had been used for treatment were washed out with 50ml of MACS buffer. The cells acquired were centrifuged at 1500rpm for 10 minutes and washed three times with MACS. The cells collected were then used for staining or gradually frozen to -80^{o}C in freezing media (10% DMSO (Sigma) with FCS (BioSera)).

Flow Cytometric Analysis of Stem Cell Grafts and PBMC

All day 2, 7 and 14 blood samples were analysed fresh. Some stem bags and healthy donors were analysed from frozen. Cells were surface stained for 30 minutes with antibodies conjugated to individual fluorochromes (see panels below) on ice and protected from light. Following incubation cells were then washed twice with MACS buffer and resuspended in 200ul MACS buffer for flow analysis. Propidium iodide was added just prior to the running of each sample in order to identify and exclude dead cells from the analysis Unstained cells were used to set voltages on the flow cytometer and single colour stained bead controls were used for compensation in each individual experiment. All data was acquired on a BD LSR II flow cytometer as lasers excited the flurophores and the emission produced was detected. The data collected was analysed using BD FACS DVIA software.

Flow panels

1. T Panel: α/β TCR (PE; Clone IP26; BioLegend), CD4 (APC-Cy7; Clone RPA-T4; BD Biosciences), CD8 (V500; Clone RPa-T8; BD Biosciences), CCR7 (APC; R&D Systems), CD45RA (AF700; Clone HI100; BioLegend), CD52 (FITC; Clone HI186; BioLegend), Propidium Iodide (PE-Texas Red; Miltenyi Biotec).

2. B Panel: CD14 (Pacific Blue; Clone 6ID3; eBioscience), CD3 (Pacific Blue; Clone OKT3; eBioscience), CD56 (Pacific Blue; Clone HCD56; BioLegend), CD27 (PE; Clone LG7F9; eBioscience), IgD (PerCPCy5.5; Clone IA6-2; BioLegend), CD19 (PE-Cy7; Clone SJ25C1; eBioscience), CD38 (APC; Clone HIT2; eBioscience), CD45 (AF700; Clone HI30; BioLegend), CD24 (APC-Cy7; Clone SN3AS-2H10; eBioscience), CD52 (FITC; Clone HI186; BioLegend), Propidium Iodide (PE-Texas Red; Miltenyi Biotec).
3. DC Panel: CD11 (PE-Cy7; Clone B-ly6; BD Biosciences), CD45 (APC-H7; Clone 2DI; BD Biosciences), HLA-DR (PerCP Cy5.5; Clone G46-6; BD Biosciences), CD80 (FITC; BD Biosciences), CD86 (APC; BD Biosciences), CD83 (PE; BD Biosciences), Propidium Iodide (PE-Texas Red; Miltenyi Biotec).
4. NK Panel: CD3 (Qdot655; Clone S4.1; Invitrogen), CD56 (APC-Cy7; Clone HCD56; BioLegend), CD16 (V500; Clone 3G8; BD Biosciences), CD57 (Pacific Blue; Clone HCD57; BioLegend), CD158a (PC5.5; Beckman Coulter), CD158b (PE-Cy7; Beckman Coulter), CD158e (AF700; Clone DX9; BioLegend), CD159a/NKG2A (APC; Beckman Coulter), NKG2C (PE; R&D Systems), CD52 (FITC; Clone HI186; BioLegend), Propidium Iodide (PE-Texas Red; Miltenyi Biotec).

Peripheral blood lymphocyte Counts

Whole blood lymphocyte counts were determined using two methods; a) BD Trucount tubes and b) Accuri flow cytometric analysis.

For Trucount analysis 20µl MACS buffer was mixed with 50µl of whole blood before addition of 450µl FACS lysing solution to the Trucount tubes. Roughly 4000 bead events were then acquired on the BD LSR II flow cyometer and cell counts analysed offline using

Diva software. The equation below was then used to calculate cell count via the Trucount method:

$$\frac{(\text{Number of cells gated} \times \text{Total number of beads in tube})}{(\text{Number of beads gated} \times \text{Test volume})} \times 10.4 \text{ (dilution factor)} = \text{cells per } \mu\text{l of blood}$$

For Accuri analysis serial dilutions of whole blood were made in MACS buffer (1/1000, 1/2000, 1/4000 and 1/8000 samples in duplicate). 50µl of each sample was then acquired on the Accuri flow cytometer after which cell counts in the lymphocyte gate were determined using Accuri analysis software. The number of lymphocytes acquired was multiplied by the dilution factor, and an average of the dilutions taken as the total lymphocyte count.

Analysis of the effects of CAMPATH *in vitro* on T cell and NK cell death

PBMC taken from peripheral blood of healthy donors were resuspended at $1x10^6$ cells/ml in RMPI, supplemented with 10% human serum. Aliquots of 100µl were then divided into sterile FACS tubes to give ~100,000 cells per test. A range of CAMPATH concentrations were applied to the cells from 20µg/ml to 0.625µg/ml, which were then incubated for three hours at 37 ^{0}C and 5% CO_2. The cells were then washed twice in MACS buffer and surface stained with one of the panels below for 30 minutes on ice, whilst protected from light. Following incubation, cells were washed twice with MACS buffer and resuspended in 200ul buffer for analysis by flow. Finally CALTAG counting beads (Invitrogen) and the PI stain were added before performing flow on the BD LSR II. Analysis was performed using BD FACS DVIA software.

Total cell counts were calculated using the below equation:

$$\frac{\text{Number of Cells Gated}}{\text{Number of Beads Gated}} \times \text{number of CALTAG counting beads per } \mu l = \text{cells per } \mu l$$

Flow panels:

1. CD3 (APC-Cy7; Clone SK7; BD Biosciences), CD56 (PE-Cy7; Clone MEM-188; BioLegend), CD52 (FITC; Clone HI186; BioLegend), PI (Texas Red; Miltenyi Biotec).
2. CD3 (PE; Beckman Coulter), CD56 (APC-Cy7; Clone HCD56; BioLegend), CD52 (FITC; Clone HI186; BioLegend), PI (Texas Red; Miltenyi Biotec).

Results

Gating Strategy

In order to analyse the large amount of data produced by running the samples through the flow cytometer a gating strategy to pull out the cell populations was required. Due to the cell markers applied this is a straightforward process but requires manual setting of the gates. Initially the live lymphocytes were identified (Figure 3) from which analysis of the individual lymphocyte populations of T cells (Figure 4), B cells (Figure 5) and NK cells (Figure 6) could progress. The T cell panel allowed identification of CD4 and CD8 T cells as well as sub populations of naïve, effector, effector memory RA and central memory cells. The B cell panel identified naïve, IgD class switched memory, IgD non-class switched memory and transitional B cells as well as plasmablasts. Finally the NK panel identified CD56 bright and dim cells as well as cells which were positive for any of the three KIR family receptors, CD158a, CD158b and CD158e. Five other cell markers were also identified on the NK cells.

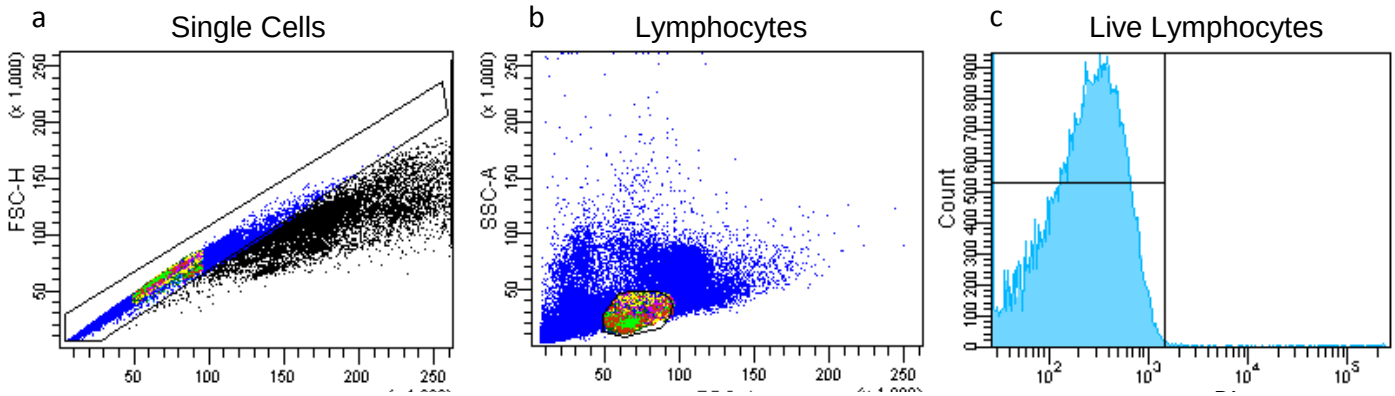

Figure 3 –Gating strategy for lymphocyte populations

To identify single cells over doublets or cell clumps, which could consist of multiple cell types, (a) a scatter plot of forward scatter height (FSC-H) against forward scatter area (SSC-A) was used to exclude larger cells. Single cells were then visualised on (b) a scatter plot of forward scatter area (FSC-A) against side scatter area (SSC-A) allowing selection of the general lymphocyte or dendritic cell population. To then exclude dead cells from the analysis a histogram of the intensity of propidium iodide (PI) of the cells was produced (c) and PI negative cells, which are live, were gated for. This gating strategy provided a populations of single, live lymphocytes after which analysis of the individual lymphocyte populations of T cells, B cells, NK cells and DC's could be carried out.

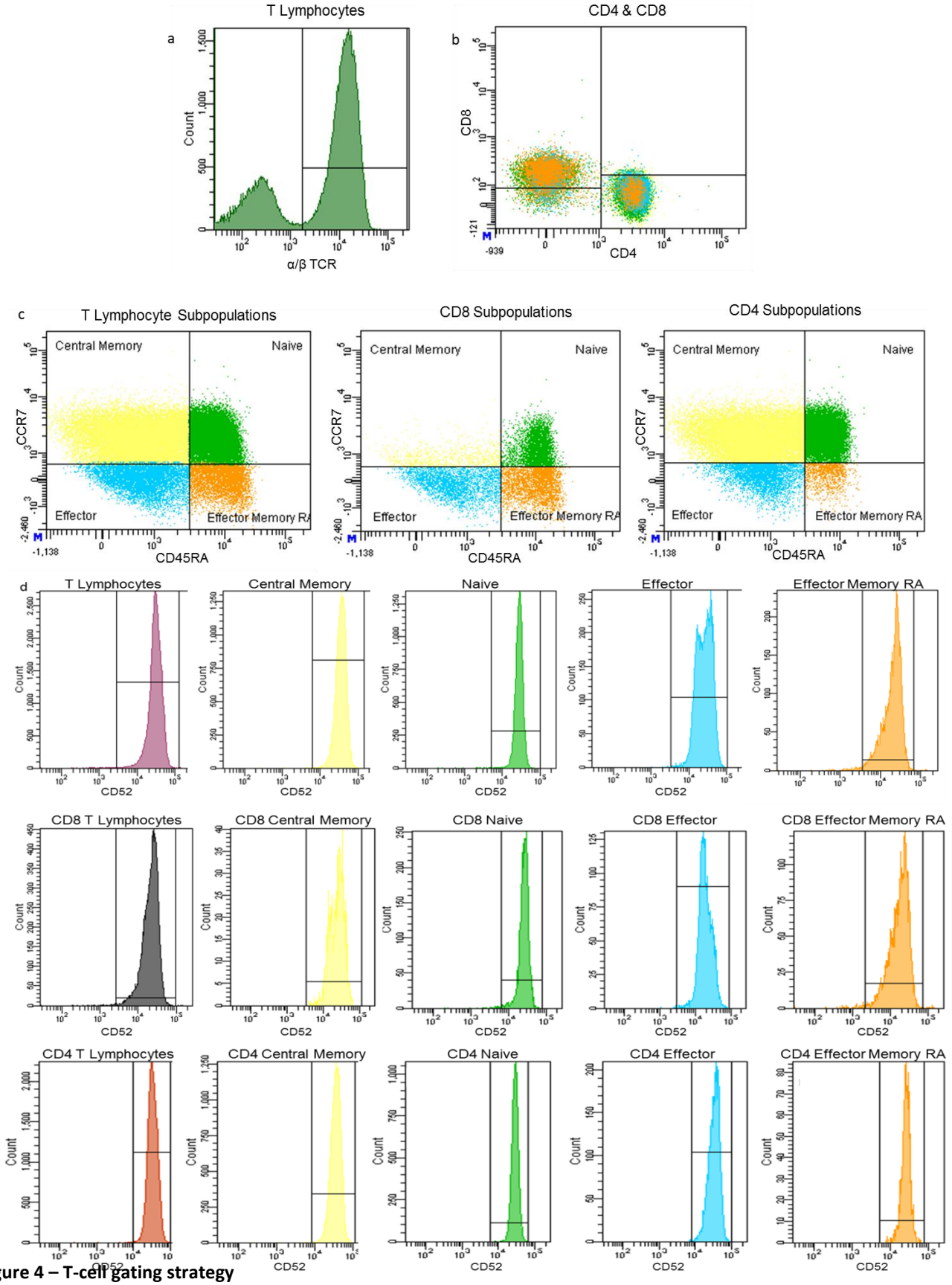

Figure 4 – T-cell gating strategy

T cells were selected by gating on cells positive for the α/β TCR-PE (part of T cell receptor complex)(a). T cells were then divided into the CD4 and CD8 subsets using a scatter plot with a quadrant gate to identify $CD4^{+}CD8^{-}$ Th cells and $CD4^{-}CD8^{+}$ CTLs (b). These subsets were then divided again, using a CD45RA against CCR7 scatter plot (c), into effector T cells (CD45RA- CCR7-), central memory T cells (CD45RA- CCR7+), effector memory T cells (CD45RA+ CCR7-) and naive T cells (CD45RA+ CCR7+). Each individual subset was then also analysed for CD52 mean fluorescence intensity (MFI) of the cells (d).

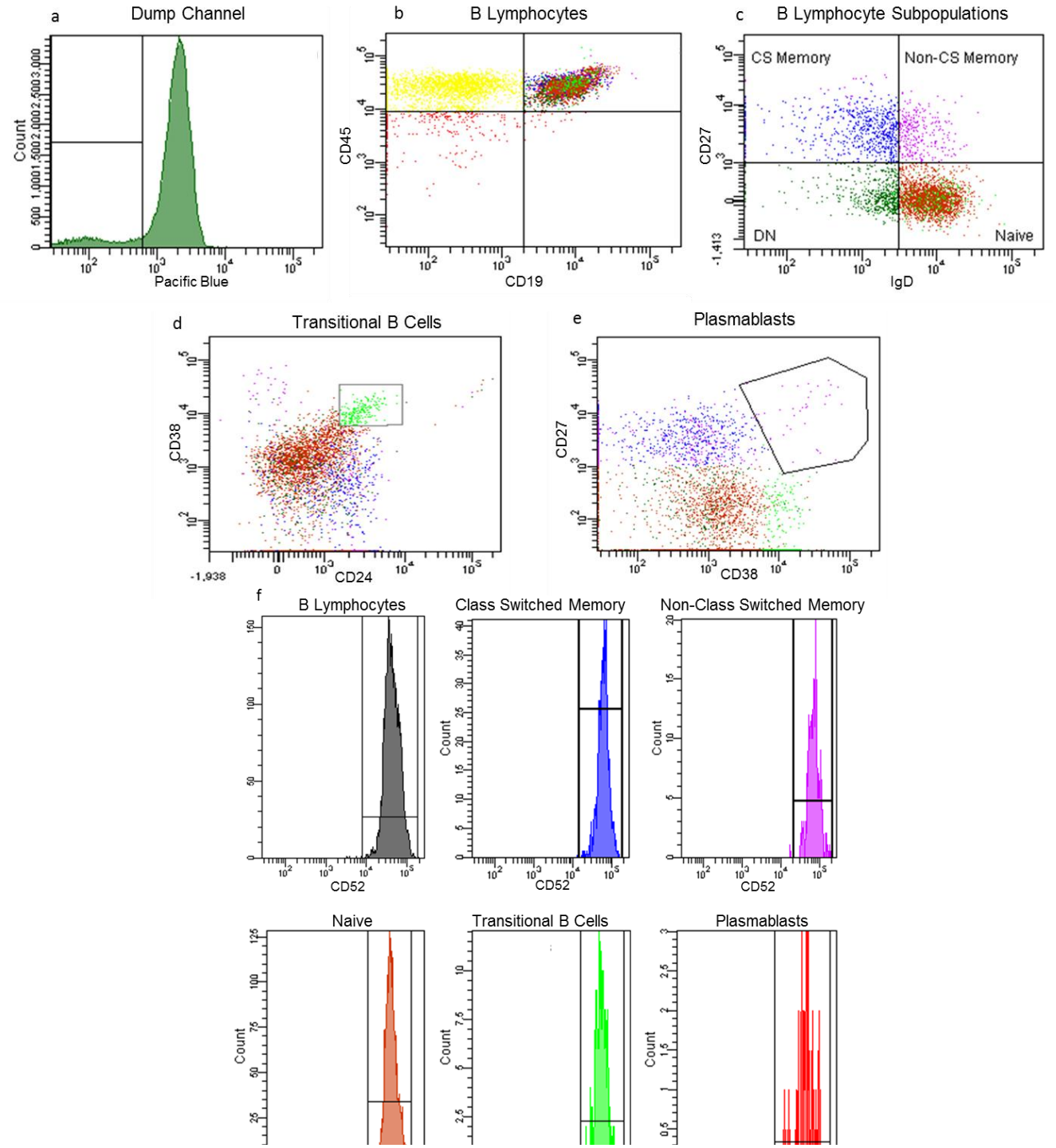

Figure 5 – B cell gating strategy

The B cell panel contained an additional dump channel where CD14, CD3 and CD56 were all conjugated to pacific blue (PB) allowing exclusion of monocytes/macrophages, T cells or NK cells respectively by gating on PB negative cells (a). To then identify B cells a double positive gate on a CD19 against CD45 scatter plot was used (b). B cells were then subdivided into immunoglobulin class switched memory B cells (CD27+IgD-), non-switched memory B cells (CD27+IgD+), and naïve B cells (CD27-IgD+) by visualising IgD against CD27 as a scatter plot (c). To gate for transitional B cells a scatter plot of CD24 against CD38 was used with a gate on the brightest double positive cells (d). Finally to identify plasmablasts a CD38 against CD27 scatter plot was used, again gating on the brightest double positive cells (e). CD52 intensity was also measured on all subsets of B cells (f). CS – class switched, DN – double negative.

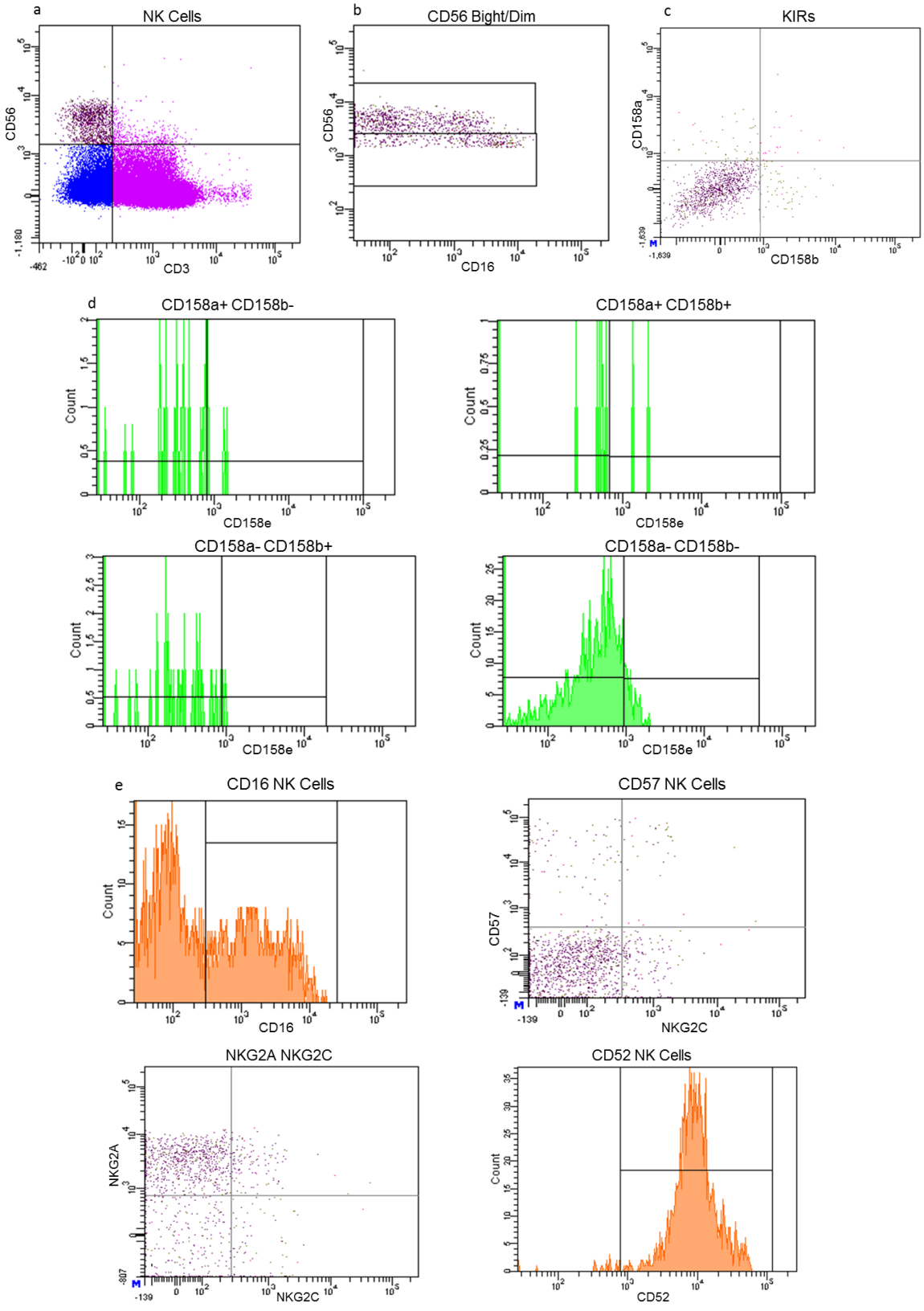

Figure 6- Natural Killer cell gating strategy

Natural killer cells were identified as CD3-CD56+ using a CD3 against CD56 scatter plot (a). NK cells were then subdivided into CD56 bright and CD56 dim NK cells (b). NK cells which possess single, double or triple positive KIRs on their surface were also determined using a scatter plot of CD158a against CD158b(c) by applying a quadrant gate to determine the absence or presence of CD158a and/or CD158b followed by analysis of CD158e using a histogram (for each quadrant analysed) and gating for positive and negative cells (d). CD16+, CD57+, NKG2A+, NKG2C+ and CD52+ NK cells were also identified (e).

Stem Cell Bag Cell Populations

The standard percentages of lymphocytes in a healthy donor are 70-75% T cells, 15-20% B cells and 10-15% NK cells. Our gating strategy provided a lymphocyte population containing 65% T Cells and 10% NK cells in the healthy donors (Figure 7a) indicating that the ratio of cells was normal although the gate was not entirely lymphocyte pure. B Cells had an additional gate to exclude monocytes/macrophages, T cells and NK cells but still only produced a 15-20% population of B cells following this exclusion, suggesting that it was not an effective way to purify out the B cells. The stem cell bag cell population was greatly different however in terms of T and B lymphocyte populations. The T cell population was down to 40% while the B cell population rose to nearly 60%, these both showed a statistically significant difference to the values found in healthy donors. NK cells however did seem to be reduced with a mean percentage of 5%, but this was not a significant difference.

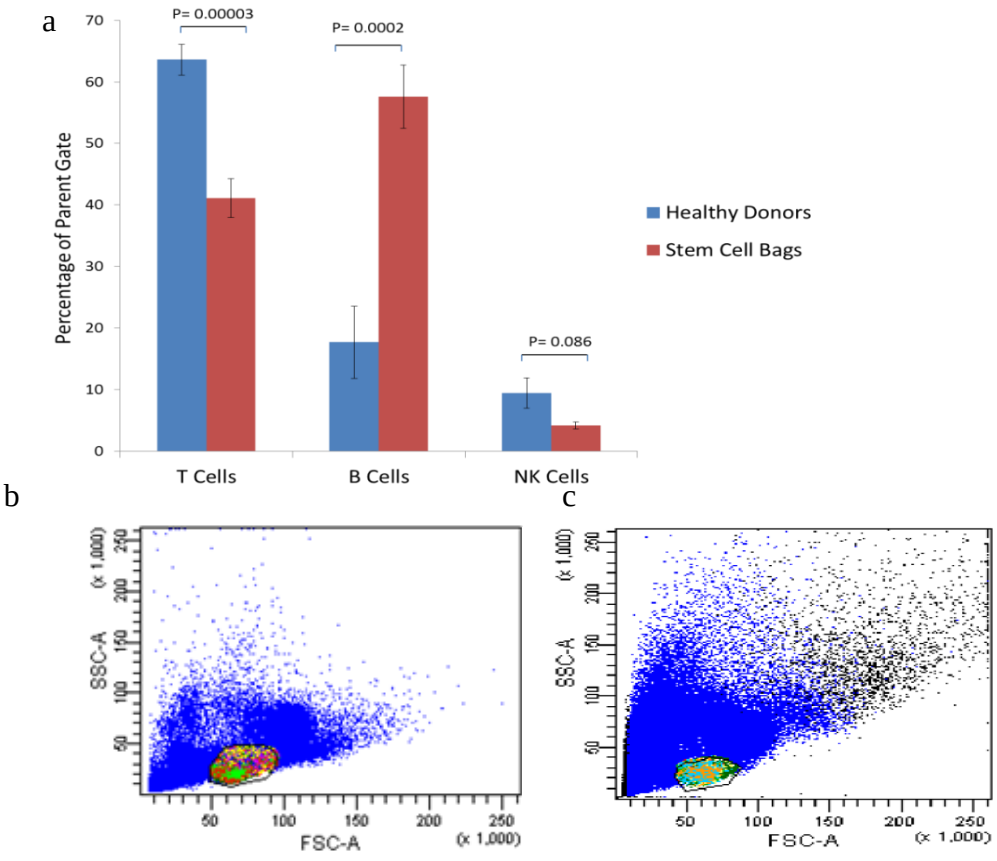

Figure 7 – Analysis of global cell populations in stem cell bags
PBMC from healthy donors and stem cell bag samples were stained with fluorochrome conjugated antibodies and cell types were determined by flow cytometry. Global populations of T and NK cells were measured as a percentage of the lymphocyte gate whilst B cells were measured as a percentage of CD3-CD14-CD56- cells found in the lymphocyte gate (a). (Healthy donors: n = 6, Stem cell bags T and B: n = 13, NK: n = 10). Lymphocyte gates on healthy donor (b) and stem bag samples (c).

The numbers of CD4 and CD8 T cells changed dramatically between healthy donors and stem bags with P values of 0.001 in both instances (Figure 8a). CD8 cells were roughly three times more prevalent than CD4 in healthy donors but in stem cell bags this had changed to a roughly even split with a P value of 0.91 indicating there was no difference in numbers of CD8 and CD4 T cells in the stem bag. When the subgroups of T cells within the CD4+ and CD8+ populations were looked at (Figures 8b and 8c) most showed no statistically significant difference apart from the CD8+ effector memory RA group which increased in percentage of the CD8 population.

Both the B cell and NK cell subgroups (Figure 8d and 8e) showed little change in their percentages. Most were statistically unchanged with only the plasmablasts seeming to decrease in the B cell panel while in the NK panel the KIR negative percentage increased as the KIR positive and CD16 positive cell populations decreased.

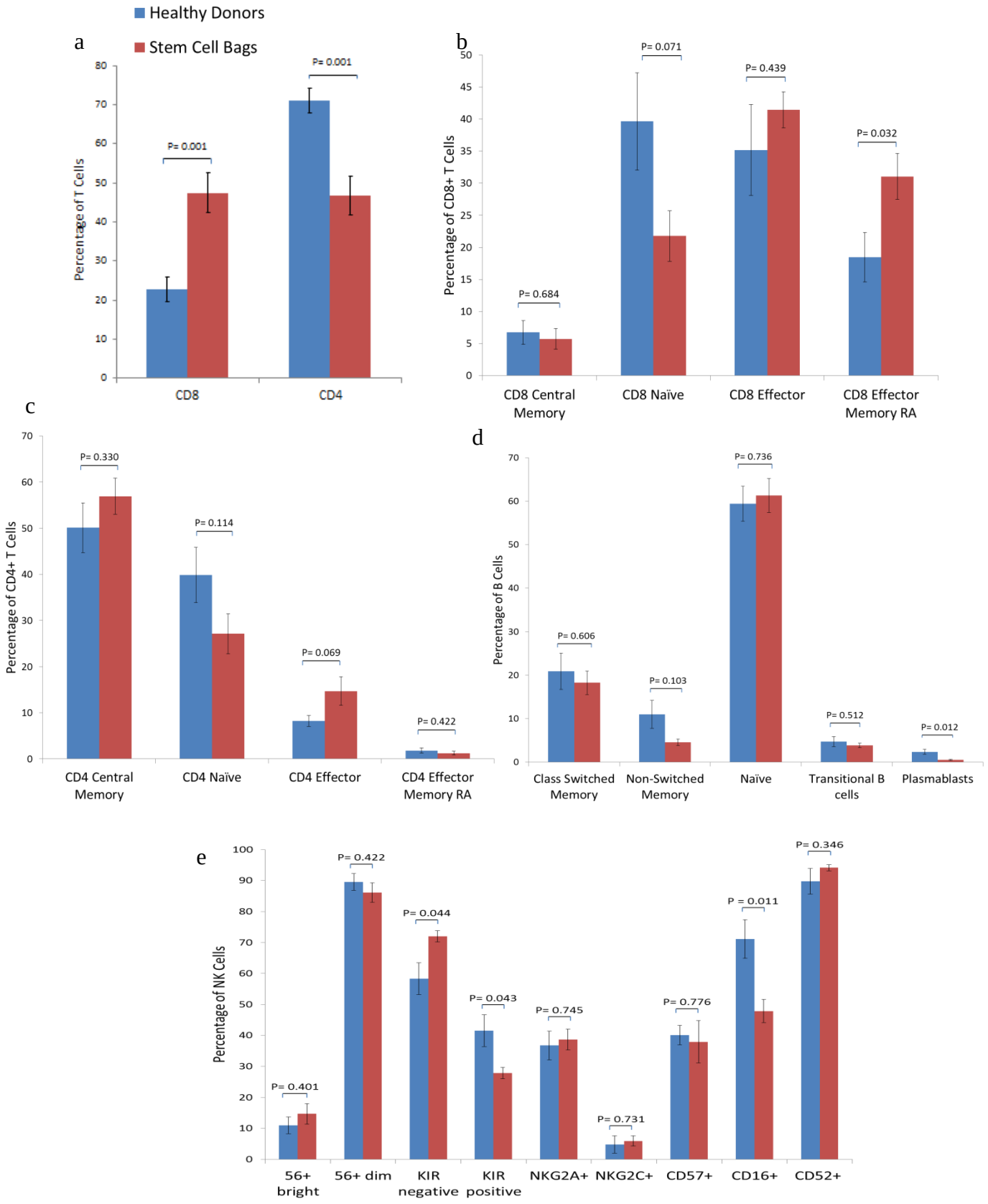

Figure 8 – Subgroup cell populations in stem cell bags
PBMC from healthy donors and stem cell bag samples were stained with fluorochrome conjugated antibodies and then cell types were determined by flow cytometry. Cells were measured as a percentage of their parent gate, either T Cells (a), CD8+ T Cells (b), CD4+ T Cells (c), B Cells (d) or NK cells (e). Healthy donors n=6, Stem cell bags T and B cells n=13, NK cells n = 10.

Stem Cell Bag CD52 Intensities

CD52 density on healthy donor cells is highest on B cells, then T cells and lowest on NK cells (Rao et al., 2012). We measured CD52 mean fluorescence intensity (MFI) as a percentage of the MFI found on the single colour control bead for CD52 from each experiment in order to standardise the results. Our data on the global cell populations corroborates with current findings as in the healthy donors B cell CD52 density was highest compared to T cell and NK, however a P value of 0.06 means there was not actually a statistically significant difference between B and T cells unless a Bonferroni correction was applied (Figure 9a). A difference is likely to be found with a higher n value of healthy donors though (n=6). In comparison to the healthy donors the stem cell bags showed the same ratio between T, B and NK cell CD52 densities however the T and B lymphocytes showed significantly lower CD52 levels when compared directly to healthy donors with P values of 0.019 and 0.036 respectively. NK cell CD52 levels remained the same between healthy donors and stem cell bags.

To determine if these differences could be attributed to changes in specific types of cells we investigated the CD52 levels on the cell subgroups. In T cells there was a significant decrease seen in both overall CD8 and CD4 cells (P values 0.031 and 0.038 respectively) as well as a seemingly universal decrease of CD52 density on stem bag cells compared to healthy donors from all the subgroups (Figure 9b). Whilst this was true for all the CD4 subgroups only the CD8 effector cells showed a statistically significant reduction. The B cells also seemed to show a universal decrease however only the memory and transitional B cells were found to be significantly reduced (Figure 9c). Finally in the NK cells none of the subgroups were found to be significantly different from the healthy donors (Figure 9d).

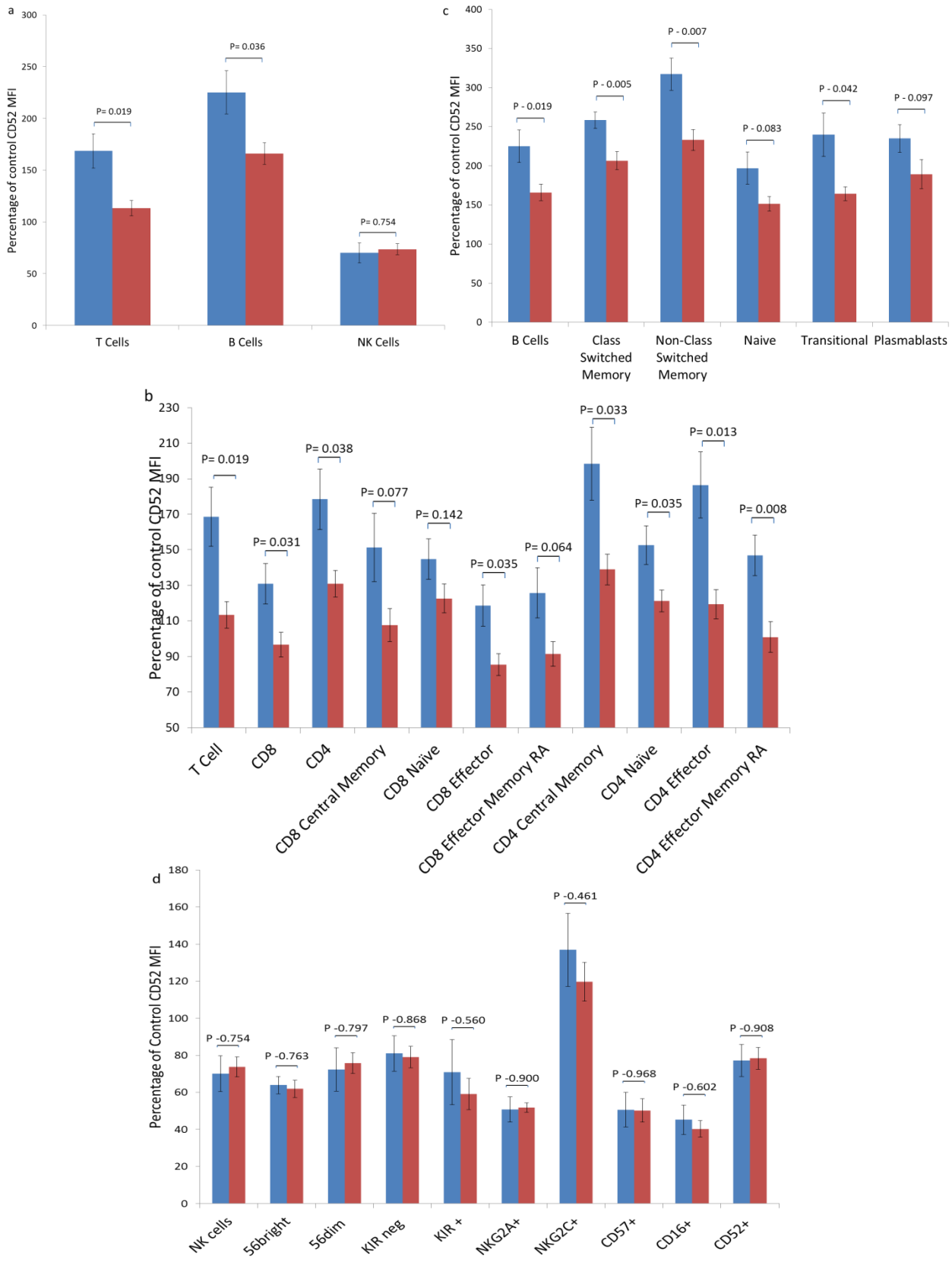

Figure 9 – Stem bag cell population CD52 intensities
CD52 MFI was measured as a percentage of the MFI found on the single colour control bead for CD52 in each experiment in order to standardise the results. This was done for global cell populations (a) as well as the individual subgroups of T cells (b), B cells (c) and NK cells (d).

Patient ID	Patient Sex	Donor Sex	Donor	Age	Disease	Campath Y/N	Campath dose	Conditioning
BW600	M	M	MUD	66	Myelodysplastic Syndrome	Y	10mgx5	FMC
IP601	M	F	MUD	34	Acute Lymphoblastic Leukaemia	Y	10mgx5	Cyclo/TBI
FN603	F	M	MUD	56	Acute Myeloid Leukaemia	Y	10mgx5	FMC
PC604	M	M	Sib	55	Non-Hodgkin's Lymphoma	Y	10mgx5	FMC
AC605	M	F	Sib	17	Aplastic Anaemia	Y	10mgx5	Cyclo/Campath
NG606	F	M	MUD	32	Hodgkin's Lymphoma	Y	10mgx5	Beam/Campath
SC607	M	F	Sib	48	Aplastic Anaemia	Y	14mg x5	Flu/Cyclo/Campath
EE608	F	M	MUD	43	Acute Lymphoblastic Leukaemia	Y	10mg x 5	Cyclo/TBI
AH609	M	M	MUD	53	Acute Myeloid Leukaemia	Y	10mgx5	FMC
JS610	F	M	Sib	54	Acute Myeloid Leukaemia	Y	10mg x 5	FMC

Table 1 – Patient information
Patients in this cohort all underwent an allogeneic haematopoietic stem cell transplant at the Queen Elizabeth Hospital Birmingham.
Definitions: Sib – Sibling; MUD – Matched Unrelated Donor; FMC -Fludarabine, Melphalan, and Campath; Cyclo – Cyclophosphamide; TBI – Total Body Irradiation; BEAM - BiCNU, Etoposide, Ara-C and Melphalan.

Early Reconstitution Cell Populations

With donor stem cells entering the patient at day 0 this gives an indication of how the cellular profile of the patient should look at that point. Collecting blood samples at day 2, day 7 and day 14 allows a time course to be built up of the cell population percentage changes and total lymphocyte count over the first two weeks post-transplant. This was done with ten patients (see Table 1) using the same methods to identify T, B and NK cells as previously. However the recovery of B cells was too low to obtain results from.

Globally T, B and NK cells are all reduced drastically following transplantation. As a percentage of the lymphocyte gate (Figure 10a) T cells fall to around 10% at day two and fail to increase by day 14. NK cells on the other hand have a much greater recovery and increase their percentage of the lymphocyte gate to greater than 20% by day seven, indicating there are more NK lymphocytes present than T cells after the first week post-transplant. The total lymphocyte count was around 15 per μl of blood (Figure 10b), a huge decrease from the healthy donor value of around 2000 per μl of blood. By day 7 this slightly increased to around 22 per μl of blood although this was not a statistically significant change. A larger increase in the second week put the lymphocyte count at around 140 per μl of blood by day 14 (P value 0.006). In terms of T cell numbers there was not a significant change as the amount stayed in the range of 1-4 T lymphocytes per μl of blood for the two week period (Figure 10c). The NK cells on the other hand showed an increase from 1 NK cell to around 23 NK cells per μl of blood from day 2 to day 14 with a P value of 0.047 (Figure 10d).

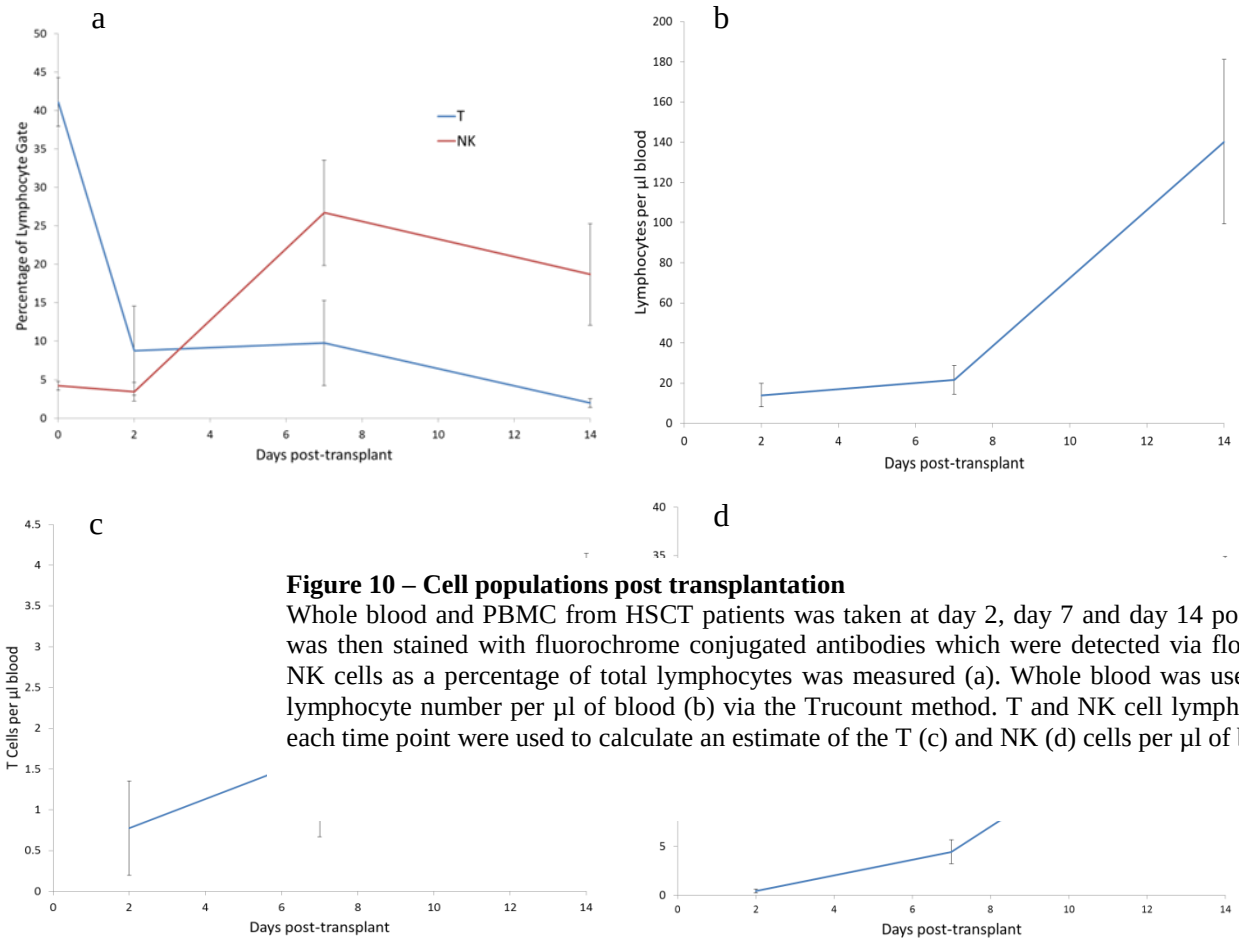

Figure 10 – Cell populations post transplantation
Whole blood and PBMC from HSCT patients was taken at day 2, day 7 and day 14 post transplant. was then stained with fluorochrome conjugated antibodies which were detected via flow cytometry. NK cells as a percentage of total lymphocytes was measured (a). Whole blood was used to measure lymphocyte number per µl of blood (b) via the Trucount method. T and NK cell lymphocyte percenta each time point were used to calculate an estimate of the T (c) and NK (d) cells per µl of blood.

Looking at T cells specifically there was a far greater reduction of CD4 cells than CD8 as is seen by a decrease in CD4 percentage and increase in CD8 percentage of the T cells remaining during VEIR (Figure 11a). Naïve and effector memory cells seem to be affected more so in CD8 positive T lymphocytes as their percentages decreased, whilst central memory and effector T cells increased in percentage by day 14 (Figure 11b). The profile of CD4 T cells stayed relatively similar following transplantation (Figure 11c). Central memory cells remained the dominant cell type and whilst naïve cells seemed to fluctuate there was no significant difference. Effector and effector memory cells seemed to be the most affected as they were not detected at day 2. However they both recovered to similar day 0 percentages by

day 14. The NK subgroup profile stayed fairly constant through the first two weeks with large variations but only four statistically significant changes compared to stem cell bags (Figure 11d, e and f). At day 7 there was an increase in CD56+ bright cell percentage (P= 0.001) and therefore also a decrease in CD56+ dim cell percentage (P= 0.002). An increase in NKG2A+ cell percentage was also seen at day 7 (P= 0.003) as well as an increase in CD16+ cells at day 2 (P= 0.026). By day 14 however there were no longer any significantly different changes in NK cell population percentages compared to stem cell bags.

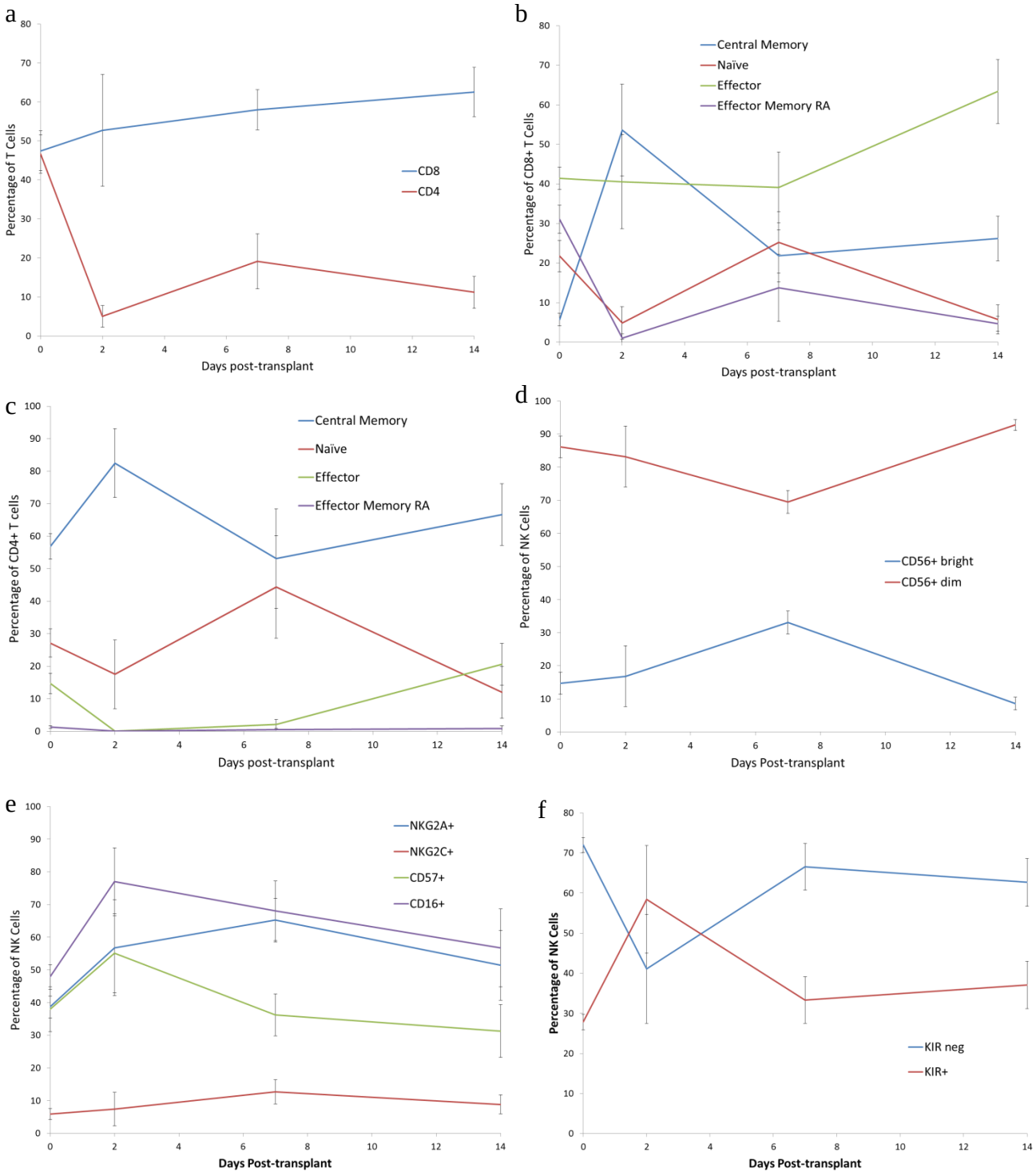

Figure 11 – Cell subpopulations during early reconstitution
PBMC from HSCT patients was taken at day 2, day 7 and day 14 post transplant and was then stained with fluorochrome conjugated antibodies. Cell types were determined by flow cytometry. Time courses of CD8 and CD4 cells (a) as well as individual CD8 (b), CD4 (c) and NK cell (d, e and f) subgroups were detected.

Early Reconstitution Cell CD52 Intensities

To detect the effect campath had on the patients during VEIR we measured CD52 intensities on each cell population. Overall both T and NK lymphocytes had dropped in CD52 intensity to roughly 20% of the control CD52 MFI at day two (Figure 12a). It seemed they had both started to recover by two weeks however this was only proven statistically in T cells at day 14 (P=0.045), which had risen to around 40% of the control CD52 MFI. All the T cell subgroups were significantly reduced in CD52 levels at day 2 with only CD8 central memory cells making a statistically significant increase by day 14 (P= 0.014) (Figure 12b). CD4 subset cells were not always found in the samples and so the n values were down to two or three making the results from them unreliable. The NK subgroups were also all significantly decreased in CD52 intensity by day 2 and despite a general recovery trend only bright CD56 positive cells showed a statistically significant increase by day 14 (P= 0.042) (Figure 12c).

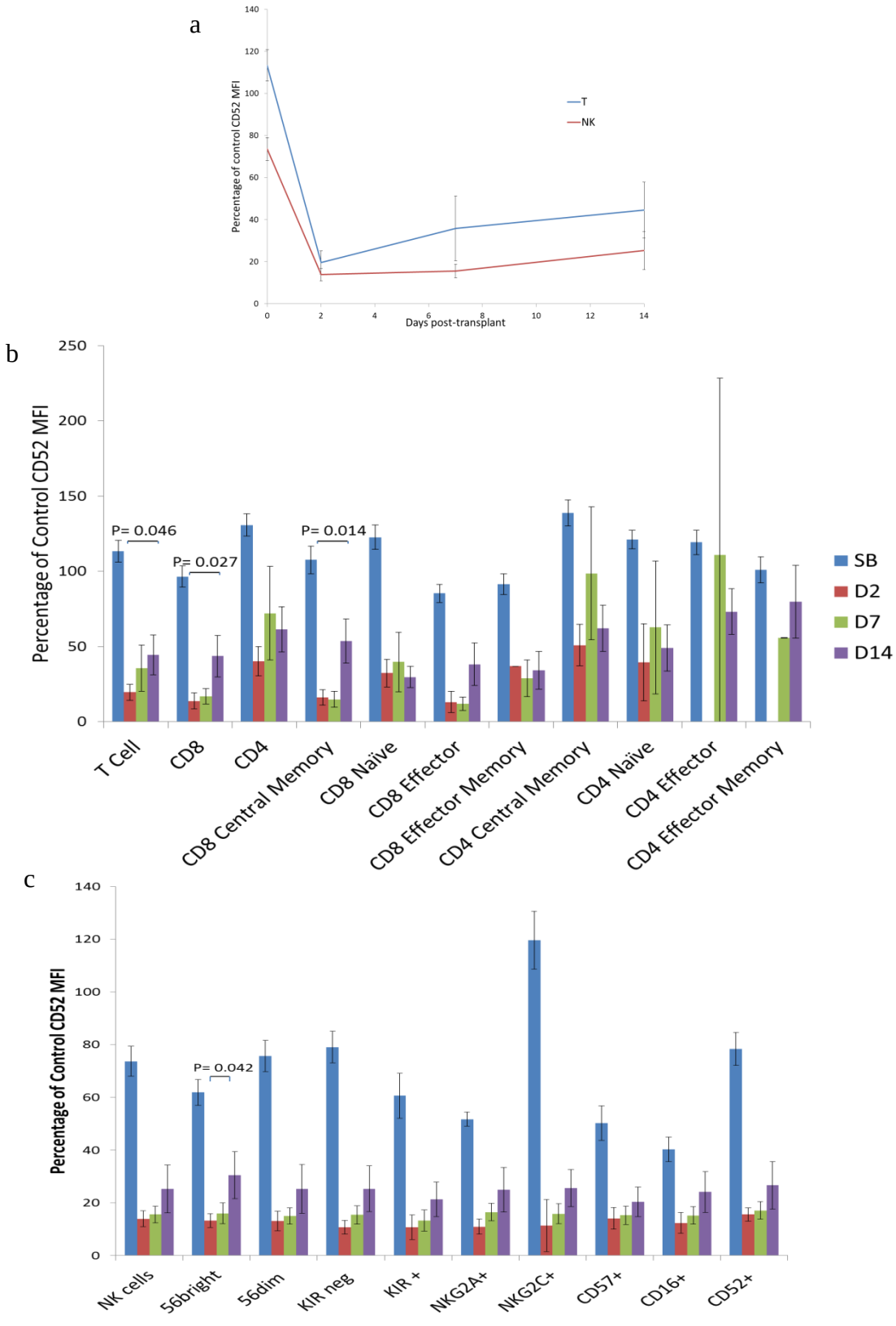

Figure 12 – CD52 intensities during early reconstitution
PBMC from HSCT patients was taken at day 2, day 7 and day 14 post transplant. PBMC was then stained with fluorochrome conjugated antibodies which were detected via flow cytometry. CD52 levels were measured as a percentage of the CD52 control MFI. This was done globally for T and NK cells (a) and for each subpopulation of the T cells (b) and NK cells (c).

Effects of CAMPATH *in vitro*

As we have seen that campath seems to be involved in the effective reduction of T and NK cells in patients we aimed to replicate the work of Rao et al. (2012), and progress from it to test the functionality of campath on stem cell bag cells and post-transplant patient samples in vitro. Therefore we first had to optimise a protocol using healthy donors. A suitable titration range was chosen from 625 ng/ml to 10,000ng/ml of campath due to work done by Spyridonidis et al (2010) which looked at average serum peak levels following different patient dosages of campath. Patients given a high dose of 20mg per day for five days had an average peak serum level of 13700 ng/ml which remained above 1000 ng/ml for at least four weeks. Patients given 10mg per day for five days, which is the dose given at the QE, resulted in an average serum peak level of 2500 ng/ml that remained above 500ng/ml for at least 11 days after the last dose. Finally patients given a low dose of 5mg per day for two days had an average peak lower than 2500 ng/ml but still in the lymphotoxic range.

Healthy donor PBMC samples were incubated with campath for three hours, in triplicate before antibodies were added, CD3 to detect T cells and CD56 to detect NK cells. A CD52 marker was also added to measure CD52 levels on the cells as well as PI to detect cell death.

Comparison of live lymphocytes as a percentage of the number found in the lymphocyte gate of the no campath control showed that there was a significant reduction in total lymphocyte numbers due to the incubation (P=0.033), which was increased by the addition of camapth, even at the lowest dose (Figure 13a). Lymphocyte numbers dropped around 10% with the incubation and by an additional 15% with the 625 ng/ml dose of campath. This increased to around 30% with the highest dose of 10,000 ng/ml. Looking individually at the T cell population in the lymphocyte gate (Figure 13b) it follows a similar pattern, which is not surprising as T cells make up the majority of the healthy donor lymphocyte population. A 5% decrease was found with incubation and further 15% with the first camapth addition, however

these were not found to be statistically significant. By the 2500 ng/ml dose the change was found to be significant (P= 0.018) with a reduction of roughly 30% of T cells with the highest dose. The NK population also decreased with campath (Figure 13c). It was reduced with the lowest dose, however the amount remained the same despite the higher concentrations of campath being added. Unusual control values in one experiment skewed the data so precise percentage decreases and statistically significant differences were not obtainable. The general trend of a decrease which remained stable despite increase campath concentrations is clear however.

Detection of T and NK cell death found a general increase in PI stained cells. However the variation between experiments meant that no significant change was actually seen in T cells (Figure 13d) and only with the highest doses was the increase found with NK cells (Figure 13e).

CD52 levels as a whole on lymphocytes decreased substantially with increased campath concentrations (Figure 13f). There was no difference between the controls indicating that it was the campath which caused the specific reduction of high density CD52 cells. The intensity dropped by around 20% with the first campath dose and was at a 60% decrease by the last. This was also seen when the T cells were taken on their own (Figure 13g) with roughly the same percentage decreases. In NK cells a general decreasing trend was also found, but without the statistical significance to confirm (Figure 13h).

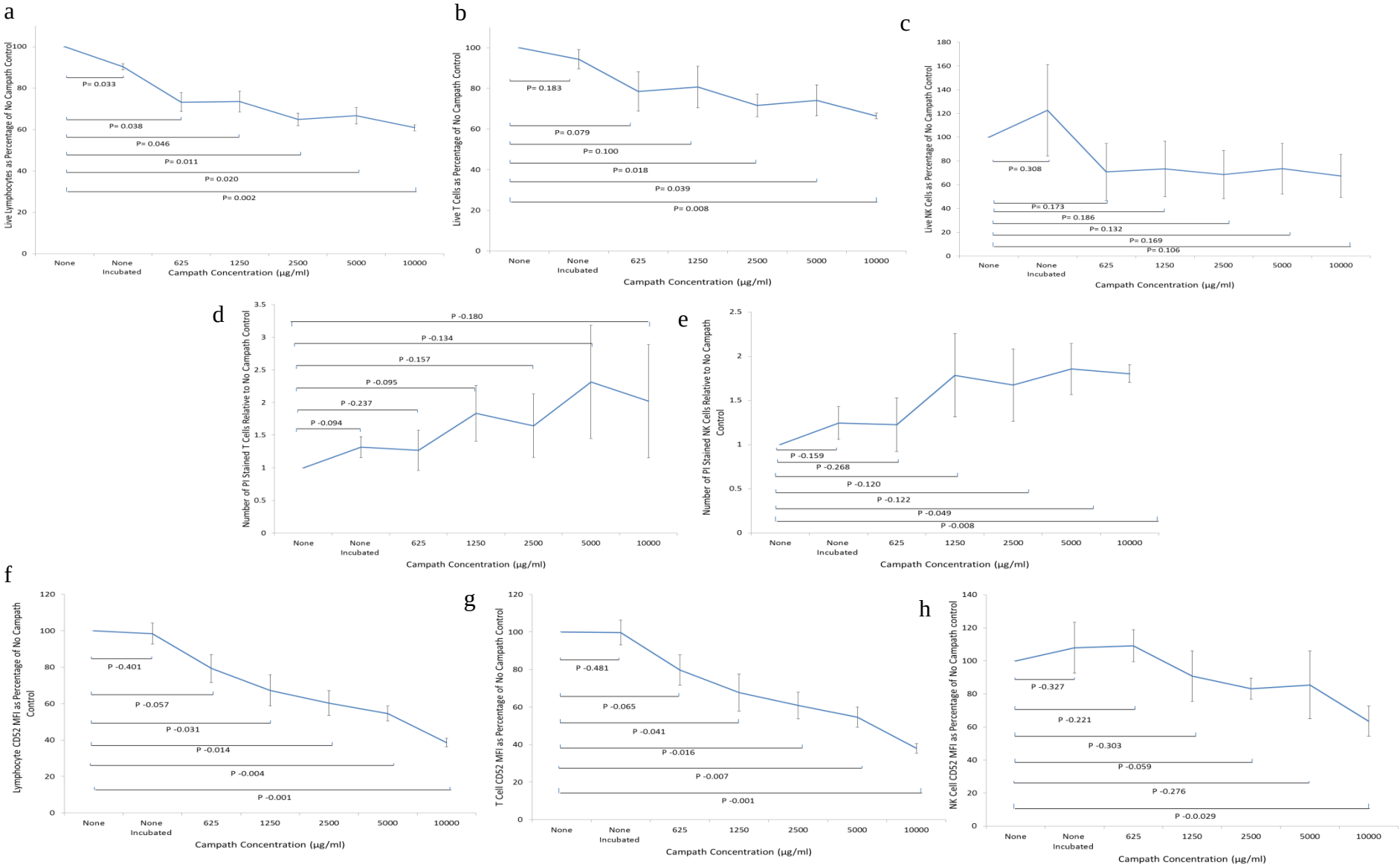

Figure 13 – Effects of Campath *in vitro* on cell death

PBMC from healthy donors was incubated for three hours at 37^0C and 5% CO_2 with a campath titration of 625 – 10,000 µg/ml. Numbers of live lymphocytes (a), T cells (b) and NK cells (c) found were represented as a percentage of the number of live cells, from each population, identified in the no campath control which was not incubated. Cell death was detected using PI and numbers of T cell (d) and NK cells (e) found with PI staining were represented relative to the no campath and no incubation control. The MFI of CD52 was measured in lymphocytes (f), T cells (g) and NK cells (h) and represented as a percentage of the CD52 MFI of the no campath and no incubation control. (n=3 for all points).

Discussion

Lymphocyte populations isolated from stem cell bags differ from healthy donor

To determine whether there were any differences in the PBMC populations between stem cell bags and healthy donors we compared the frequencies of T cell, B cell and NK cell populations between the samples, and the levels of CD52 which were expressed.

Differences were observed between the cellular populations mainly a decrease in the T cell lymphocyte gate percentage and an increase in B cells. The CD4 to CD8 percentages of T cells also changed from a predominantly CD8+ population in healthy donors to a roughly even mixture of CD8+ and CD4+ in the stem cell bags. Looking at specific T, B and NK cell types did not yield many statistically significant changes apart from increases in CD8 effector memory RA T cell percentage, KIR positive and CD16 positive NK cells as well as a decrease in plasmablasts B cell percentage. In terms of CD52 intensity the high density CD52 T and B cells were significantly dimmed in the stem cell bags compared to healthy donors whereas there was no difference seen with the NK cells. The individual subpopulations of T and B cells showed a decrease across all the cell types but was only statistically significant in a few.

The most obvious reason for these differences can either be attributed to the drug given to the donor to induce cell proliferation or due to the processing and storage of the cells before transplantation. The donor has received a five day course of G-CSF to stimulate bone marrow cell proliferation which will affect some cell more than others. T cells are affected directly, as CD4 and CD8 cells possess G-CSF receptors, and are also affected indirectly by the responses and cytokines produced by other cells

(Franzke et al., 2003). Therefore G-CSF can stimulate T cell proliferation but with alterations in T cell function. In contrast G-CSF has been shown to have limited proliferation effect on B cells in vitro, instead it is able to increase the immunoglobulin output of activated cells (Morikawa et al., 1993). This would however suggest the opposite of the results found however the global differences between T and B cell populations have to be considered carefully. Direct comparison between the frequencies may not be appropriate here due to the differences in the FSC/SSC of the stem bag and healthy donor lymphocyte populations when visualised on the flow cytometer (Figure 7b and 7c). This may be due to differing amounts of debris or other viable cells becoming included in the lymphocyte gates. Using counting beads to measure the numbers of cells present within the lymphocyte gate would allow a more direct comparison. However what we can conclude from the global data is that the ratios of T:B:NK cells, within the overall lymphocyte population, seem to be different between healthy donors and the stem bags and as the differences are substantial there is likely either a decrease in T cell number, increase in B cells or both.

The change in the CD4 to CD8 ratio of T lymphocytes in the stem cell bag compared to healthy donors may be the result of an increase of CD8 cells or a decrease of CD4 cells rather than the formation of CD4/CD8 double positive cells. It is possible for terminally differentiated CD8 or CD4 cells to acquire expression of the other however this is rare and was not seen in this instance (Parel and Chizzolini. 2004). An explanation may be made by the ability of G-CSF to activate CD4 cells (Franzke et al., 2003). Terminal differentiation and prevention of proliferation from this would decrease CD4 numbers and even out the CD4:CD8 ratio.

The decrease of plamsablasts may also be explained by the stimulation of G-CSF activating B cells and therefore stimulating plasmablasts to differentiate into mature plasma cells. The NK cell subpopulation increase of CD16 positive cells suggests a growth in the cytotoxic function of NK cells, however it has been shown that G-CSF actually downregulates NK cytotoxicity in healthy donors (Su et al., 2012). This may be due to the increase in KIR positive NK cells conferring more of a negative regulatory effect on the cells.

We observed a decrease in the level of CD52 on both T and B cells in the stem cell bags compared to health donors, whilst the level of CD52 on the surface of NK cells stayed constant. On average healthy donor T and B cells possessed more than double the CD52 intensity their surface compared to NK cells. This suggests that the CD52 level changes occurring between healthy donors and the stem bag cells only affect the high density CD52 cells. The subpopulation CD52 densities in relation to each other corroborate the data found by Rao et al, (2012). They also fit with the with the suggestion that higher intensity CD52 cells are affected more as CD4 cells expressing higher CD52 intensity were reduced more than the CD8 cells, while the memory and transitional B cells which also possess the highest CD52 values were the most affected of the B cell subpopulations. The change in CD4 to CD8 ratio may explain part of the drop in the overall T cell CD52 level as the increase of CD8 cell number or percentage would result in a CD52 drop due to the lower CD52 density on CD8 cells compared to CD4. CD8 effector memory RA cells increased in their percentage of the CD8 population while CD8 and CD4 effector cells also seemed to increase although not significantly. Activation of T cells will reduce the CD52 density of the cells which

would explain the drop in CD4 and CD8 CD52 levels. This is seen by the reduced intensity of the CD8 effector and effector memory RA cell types compared to naïve and central memory. However this doesn't explain the CD52 drop across all the subgroups indicating that either the addition of G-CSF or the processing of the stem cell bag contents is dimming all the cells.

Lymphocyte populations recover at differing rates during VEIR

To determine how cell populations recovered during VEIR we examined the frequencies of T cell, B cell and NK cell populations and the levels of CD52 which were expressed on cells with blood samples at day 2, 7 and 14 post transplantation. The numbers of B cells collected were almost beyond detection at day 2 and had not recovered to a substantial amount by day 14 to produce results from. T and NK cells were also greatly reduced at day 2 but started to recover with NK cells doing so at a faster rate and becoming the dominant lymphocyte cell type by day 14. CD8 T cells became more prevalent than CD4 T cells during VEIR. CD52 levels on both T and NK cells dropped massively with only T cells recovering significantly by day 14.

NK cells possessing greater early reconstitution ability may be attributed to their relatively lower CD52 surface density. T and B cells failed to recover to substantial levels by day 14, with the patients clearly remaining highly deficient. Their higher CD52 level of expression means they are more effectively targeted by campath (Rao et al., 2012). Campath can still act on these cells as the 10mg for five day dosage remains at lymphotoxic levels in patient serum for at least 11 days after the last dose (Rebello et al., 2001). Therefore NK cells lower surface CD52 means they are less

affected, protected from the campath conditioning and can recover faster. This effect may also explain the dominance of the CD8 positive T cells over the CD4 positive T cells as CD4 cells have a higher CD52 density than the CD8 cells, making them more susceptible to campath. The T cell subgroup data collected must however be taken cautiously as the numbers of cells involved were very limited, if any were present at all. Low n values and large variation in small numbers of cells will have skewed the data beyond reliability.

Low cell numbers are a problem when investigating VEIR, especially at day two where the maximum amount of blood that can be taken from the patient only yields very low numbers of lymphocytes, therefore exploring subgroup populations is a challenge. Low cell numbers also increase the likelihood of human error when applying the gating strategy during analysis. Selecting gates is always partially subjective but with fewer cells it is more difficult and will produce larger errors if not done accurately enough. The low numbers of cells in the whole blood post-transplant also made accurate measurement of lymphocyte number a problem. The trucount method which is validated as an accurate way to measure lymphocyte numbers works well in healthy donors where the lymphocyte numbers outweigh the beads collected, however in our patient samples where is it difficult to even identify the lymphocyte gate this method is not precise enough.

Development of an *in vitro* assay to monitor cell death by campath

To determine whether the different levels of CD52 on the surface of NK cells and T cells influences the effectiveness of campath on cell death we developed an *in vitro* model . Tests were performed on healthy donor PBMC in order to optimise a protocol

for future tests on stem cell bag and patient samples. Campath significantly reduced the lymphocyte population at the lowest dose and continued to act more effectively at higher doses. This was also seen individually in T and NK cells. CD52 levels were not affected by the incubation but were by the campath addition indicating that campath targets CD52 on cells. T cell CD52 intensity was affected at lower campath doses compared to NK cells.

It is clear that campath is able to kill a large proportion of lymphocytes, in particular T cells, by selecting high density CD52 cells even at low concentrations.

Attempts to measure cell death were relatively unsuccessful. This is likely due to the unsophisticated method of using PI staining to detect dead cells. Propidium iodide stains double stranded nucleic acids so if it is able to penetrate through a cell and reach the DNA the cell membrane must be damaged, indicating a dead or dying cell. This however did not prove to be sufficient to detect all the dead cells, although many may have just been completely destroyed and therefore not picked up on the flow cytometer.

Clinical relevance

These results have a number of clinical implications. Firstly the differences between healthy donor and stem cell bag cell populations means that cells are entering the body with a lower CD52 density than expected, and therefore the effect of campath on the cells is likely to be different. The dosage of campath given during conditioning may not be as effective as it should be and not providing as complete GvHD prevention as it could. Post-transplant the loss of B and T cells and prevalence of NK cells during VEIR is encouraging for GvHD prevention as NK cells are able to induce

a GvL effect as well as inhibit and lyse donor T cells which are activated in the initiation of GvHD (Olson et al., 2010). However low numbers of T cells will make the patient more susceptible to infections, which may require more hospitalisation and further treatment and therefore may result in more complications in the long run.

Future work

This work has shown that there is a real issue in the difference between the cell populations of a healthy donor and what is actually transplanted into a patient. In order to develop this blood samples taken from donors before addition of G-CSF as well as at the same time as the stem cell harvest would allow a direct comparison to the stem cell bag to show differences due to the drug and the processing of the cells. Measuring CD52 levels on the blood samples of donors before and after they have received their stem cell stimulation would be an interesting advancement of this.

In order to progress the campath in vitro functionality experiments we plan to use Annexin-V staining alongside PI to create a more sophisticated cell death detection method and allow the determination of different types of cell death. We will also use cell sorting to acquire purified populations of T and NK cells and test campath functionality on them directly. This could be achieved through fluorescence-activated cell sorting (FACS), however this means that the cells have been modified by the addition of an antibody which may affect the cell function. The alternative is to use magnetic activated cell sorting (MACS) and label the unwanted cells with antibodies coated in magnetic nanoparticles before feeding them through a magnetic column to leave a purified population of the cells of interest which are unmodified.

Once this has been achieved to a suitable and repeatable standard we will progress to test the campath effect on stem cell bag and VEIR patient samples. This will begin to provide information on how the overall CD52 density decrease in the stem cell bag

affects the campath functionality on those cells as well as the role campath plays post-transplant.

We have used flow cytometry to show that there are differences between the cell populations found in stem cell bags used during haematopoietic stem cell transplantation and healthy donors. These differences are likely attributed to the application of G-CSF to the donor and/or the processing of the cells during the procedure. We also witnessed the changes in T and NK cell populations during the first two weeks post transplantation during which NK cells became the dominant cell type, which is partially due to the camapth conditioning patients received pre-transplant. Finally we began development of an in vitro campath functionality protocol which found that T and NK cells are both affected at low doses of campath which targets high density CD52 cells.

References

1. Agematsu K, Hokibara S, Nagumo H, Komiyama A. (2000) CD27: a memory B-cell marker. Immunology Today. 21(5); 204–206.
2. Akbar A.N, Terry L, Timms A, Beverley P.C, Janossy G. (1988) Loss of CD45R and gain of UCHL1 reactivity is a feature of primed T cells. J Immunol. 140; 2171–2178.
3. Alberts B, Johnson A, Lewis J, Raff M, Roberts K, and Walter P. (2008) Molecular Biology of the Cell (5th edition). New York, Garland Science.
4. Blom B, Spits H. (2006) Development of human lymphoid cells. Annu Rev Immunol. 24; 287-320.
5. Caligiuri MA. (2008) Human natural killer cells. Blood. 112(3); 461-469.
6. Croudace JE, Inman CF, Abbotts BE, Nagra S, Nunnick J, Mahendra P, Craddock C, Malladi R, Moss PA. (2012) Chemokine-mediated tissue recruitment of CXCR3+ CD4+ T cells plays a major role in the pathogenesis of chronic GVHD. Blood. 120(20); 4246-4255.
7. Depoil D, Fleire S, Treanor BL, Weber M, Harwood NE, Marchbank KL, Tybulewicz VL, Batista FD. (2008) CD19 is essential for B cell activation by promoting B cell receptor-antigen microcluster formation in response to membrane-bound ligand. Nat Immunol. 9(1); 63-72.
8. Domagała A, Kurpisz M. (2001) CD52 antigen--a review. Med Sci Monit. 7(2); 325-331.
9. Ferrara JL, Levine JE, Reddy P, Holler E. (2009) Graft-versus-host disease. Lancet. 373(9674); 1550-1561.
10. Franzke A, Piao W, Lauber J, Gatzlaff P, Könecke C, Hansen W, Schmitt-Thomsen A, Hertenstein B, Buer J, Ganser A. (2003) G-CSF as immune regulator in T cells expressing the G-CSF receptor: implications for transplantation and autoimmune diseases. 102(2); 734-739.
11. Gray D. (2002) A role for antigen in the maintenance of immunological memory. Nature Reviews Immunology. 2; 60-65.
12. Hale G, Bright S, Chumbley G, Hoang T, Metcalf D, Munro AJ, Waldmann H. (1983) Removal of T cells from bone marrow for transplantation: a monoclonal antilymphocyte antibody that fixes human complement. Blood. 62(4); 873-882.
13. Holling TM, Schooten E, van Den Elsen PJ. (2004) Function and regulation of MHC class II molecules in T-lymphocytes: of mice and men. Hum Immunol. 65(4); 282-290.
14. Horowitz MM, Gale RP, Sondel PM, Goldman JM, Kersey J, Kolb HJ, Rimm AA, Ringdén O, Rozman C, Speck B, et al. (1990) Graft-versus-leukemia reactions after bone marrow transplantation. Blood. 75(3); 555-562.
15. Jaeger S, Fernandez B, Ferrier P. (2013). Epigenetic aspects of lymphocyte antigen receptor gene rearrangement or 'when stochasticity completes randomness'. Immunology. 139(2); 141-150.
16. Joseph C. Sun & Lewis L. Lanier. (2011) NK cell development, homeostasis and function: parallels with $CD8^+$ T cells. Nature Reviews Immunology. 11; 645-657.
17. Kanda J, Lopez RD, Rizzieri DA. (2011) Alemtuzumab for the prevention and treatment of graft-versus-host disease. Int J Hematol. 93(5); 586-593.

18. Kindred B. (1974) Rejection of skin grafts from different inbred strains by nude mice reconstituted with allogeneic or congenic thymus cell suspensions. European Journal of Immunology. 4(5); 388–389.
19. Lim TS, Goh JK, Mortellaro A, Lim CT, Hämmerling GJ, Ricciardi-Castagnoli P. (2012) CD80 and CD86 differentially regulate mechanical interactions of T-cells with antigen-presenting dendritic cells and B-cells. PLoS One. 7(9); e45185.
20. Ma CS, Deenick EK, Batten M, Tangye SG. (2012) The origins, function, and regulation of T follicular helper cells. J Exp Med. 209(7); 1241-1253.
21. Marijt WA, Heemskerk MH, Kloosterboer FM, Goulmy E, Kester MG, van der Hoorn MA, van Luxemburg-Heys SA, Hoogeboom M, Mutis T, Drijfhout JW, van Rood JJ, Willemze R, Falkenburg JH. (2003) Hematopoiesis-restricted minor histocompatibility antigens HA-1- or HA-2-specific T cells can induce complete remissions of relapsed leukemia. Proc Natl Acad Sci U S A. 100(5); 2742-2747.
22. Martinez FO, Sica A, Mantovani A, Locati M. (2008) Macrophage activation and polarization. Front Biosci. 13; 453-461.
23. Mei HE, Yoshida T, Muehlinghaus G, Hiepe F, Dörner T, Radbruch A, Hoyer BF. (2007) Phenotypic analysis of B-cells and plasma cells. Methods Mol Med. 136; 3-18.
24. Morikawa K, Miyawaki T, Oseko F, Morikawa S, Imai K. (1993) G-CSF enhances the immunoglobulin generation rather than the proliferation of human B lymphocytes. Eur J Haematol. 51(3); 144-151.
25. Murphy K, Travers P, Walport M & Janeway C. (2012). Janeway's Immunobiology (8th Edition), New York, Garland Science.
26. Olson JA, Leveson-Gower DB, Gill S, Baker J, Beilhack A, Negrin RS. (2010) NK cells mediate reduction of GVHD by inhibiting activated, alloreactive T cells while retaining GVT effects. Blood. 115(21); 4293-4301.
27. Parel Y, Chizzolini C. (2004) CD4+ CD8+ double positive (DP) T cells in health and disease. Autoimmun Rev. 3(3); 215-220.
28. Piper KP, Horlock C, Curnow SJ, Arrazi J, Nicholls S, Mahendra P, Craddock C, Moss PA. (2007) CXCL10-CXCR3 interactions play an important role in the pathogenesis of acute graft-versus-host disease in the skin following allogeneic stem-cell transplantation. Blood. 110(12); 3827-3832.
29. Radaev S, Sun PD. (2003) Structure and function of natural killer cell surface receptors. Annu Rev Biophys Biomol Struct. 32; 93-114.
30. Rao S.P, Sancho J, Campos-Rivera J, Boutin P.M, Severy P.B, Weeden T, Shankara S, Roberts B.L, and Kaplan J.M. (2012) Human Peripheral Blood Mononuclear Cells Exhibit Heterogeneous CD52 Expression Levels and Show Differential Sensitivity to Alemtuzumab Mediated Cytolysis. PLoS One. 7(6); e39416.
31. Rebello P, Cwynarski K, Varughese M, Eades A, Apperley JF, Hale G. (2001) Pharmacokinetics of CAMPATH-1H in BMT patients. Cytotherapy. 3(4); 261-267.
32. Reddy P. (2003) Pathophysiology of acute graft-versus-host disease. Hematol Oncol. 21(4); 149-161.
33. Reddy RL. (2005) Mobilization and collection of peripheral blood progenitor cells for transplantation. Transfus Apher Sci. 32(1); 63-72.

34. Sallusto F, Geginat J, Lanzavecchia A. (2004) Central memory and effector memory T cell subsets: function, generation, and maintenance. Annu Rev Immunol. 22; 745-763.
35. Shulman Z, Cohen SJ, Roediger B, Kalchenko V, Jain R, Grabovsky V, Klein E, Shinder V, Stoler-Barak L, Feigelson SW, Meshel T, Nurmi SM, Goldstein I, Hartley O, Gahmberg CG, Etzioni A, Weninger W, Ben-Baruch A, Alon R. (2011). Transendothelial migration of lymphocytes mediated by intraendothelial vesicle stores rather than by extracellular chemokine depots. Nat Immunol. 13(1); 67-76.
36. Sims GP, Ettinger R, Shirota Y, Yarboro CH, Illei GG, Lipsky PE. (2005) Identification and characterization of circulating human transitional B cells. Blood. 105(11); 4390-4398.
37. Smith-Garvin J.E, Koretzky G.A and Jordan M.S (2009). T Cell Activation. Annu Rev Immunol. 27; 591–619.
38. Spyridonidis A, Liga M, Triantafyllou E, Themeli M, Marangos M, Karakantza M, Zoumbos N. (2010) Pharmacokinetics and clinical activity of very low-dose alemtuzumab in transplantation for acute leukemia. Bone Marrow Transplant. 46(10); 1363-1368.
39. Su YC, Li SC, Hsu CK, Yu CC, Lin TJ, Lee CY, Liao HF. (2012) G-CSF downregulates natural killer cell-mediated cytotoxicity in donors for hematopoietic SCT. Bone Marrow Transplant. 47(1); 73-81.
40. Sugrue MW, Hutcheson CE, Fisk DD, Roberts CG, Mageed A, Wingard JR, Moreb JS. (1998) The effect of overnight storage of leukapheresis stem cell products on cell viability, recovery, and cost. J Hematother. 7(5); 431-436.
41. Torelli GF, Lucarelli B, Iori AP, De Propris MS, Capobianchi A, Barberi W, Valle V, Iannella E, Natalino F, Mercanti C, Perrone S, Gentile G, Guarini A, Foà R. (2011) The immune reconstitution after an allogeneic stem cell transplant correlates with the risk of graft-versus-host disease and cytomegalovirus infection. Leuk Res. 35(8); 1124-1126.
42. Tze LE, Horikawa K, Domaschenz H, Howard DR, Roots CM, Rigby RJ, Way DA, Ohmura-Hoshino M, Ishido S, Andoniou CE, Degli-Esposti MA, Goodnow CC. (2011) CD83 increases MHC II and CD86 on dendritic cells by opposing IL-10-driven MARCH1-mediated ubiquitination and degradation. J Exp Med. 208(1); 149-165.
43. Viret C, Janeway CA Jr. (1999). MHC and T cell development. Rev Immunogenet. 1(1); 91-104.
44. Vivier E, Tomasello E, Baratin M, Walzer T, Ugolini S. (2008) Functions of natural killer cells. Nat Immunol. 9(5); 503-510.
45. Waldmann H, Polliak A, Hale G, Or R, Cividalli G, Weiss L, Weshler Z, Samuel S, Manor D, Brautbar C, et al. (1984) Elimination of graft-versus-host disease by in-vitro depletion of alloreactive lymphocytes with a monoclonal rat anti-human lymphocyte antibody (CAMPATH-1). Lancet. 2(8401); 483-486.
46. Weisdorf D, Hakke R, Blazar B, Miller W, McGlave P, Ramsay N, Kersey J, Filipovich A. (1991) Risk factors for acute graft-versus-host disease in histocompatible donor bone marrow transplantation. Transplantation. 51(6); 1197-1203.

Acknowledgements
Dr Joanne Croudace

Dr Charlotte Inman
Tracey Chan